Digital Comprehensive Summaries of Uppsala Dissertations
from the Faculty of Science and Technology 2349

Innovative seismic imaging solutions

From hardrock mineral exploration to quick-clay site characterization

TATIANA PERTUZ

ACTA UNIVERSITATIS
UPSALIENSIS
2024

ISSN 1651-6214
ISBN 978-91-513-1988-9
urn:nbn:se:uu:diva-517419

UPPSALA
UNIVERSITET

Dissertation presented at Uppsala University to be publicly examined in Hambergsalen, Villavägen 16, Uppsala, Friday, 2 February 2024 at 10:00 for the degree of Doctor of Philosophy. The examination will be conducted in English. Faculty examiner: Prof. Dr. Cesare Comina (University of Turin).

Abstract

Pertuz, T. 2024. Innovative seismic imaging solutions. *From hardrock mineral exploration to quick-clay site characterization*. *Digital Comprehensive Summaries of Uppsala Dissertations from the Faculty of Science and Technology* 2349. 76 pp. Uppsala: Acta Universitatis Upsaliensis. ISBN 978-91-513-1988-9.

Seismic methods are an efficient and powerful tool to explore the subsurface. It principally helps to gain information on the subsurface structure, bedrock topography, and the nature of the host rock. This thesis showcases two sites in Sweden, where their geological setting, rock structure and geological environment are different, but seismic still shows its potential in soil investigation.

The first case application was in Blötberget mine, where there is an iron-oxide deposit of high-quality. It was tested the validity of an electromagnetic vibrator (E-Vib) as a seismic source for a hardrock environment, and applied a tailored processing workflow to the seismic data to image the iron-oxide deposit.

The second case study was in Lilla Edet city, where there is the presence of quick-clays in the region. From this seismic dataset, it was retrieved a S-wave reflection section from a vertical-impact source recorded on vertical-component. In the same study area, it was also imaged the P-P and S-S wavefield reflections from a 9C dataset. This provided insight on the benefit of 9C seismic data acquisition for quick-clay landslide studies.

Findings of this work prove that the E-Vib test at the Blötberget mine (Sweden) validated its effectiveness and quality for the hardrock environment. The broadband source combined with a tailored processing workflow allowed imaging of the iron-oxide deposits in improved resolution compared to the earlier seismic data. The seismic dataset in the second case study, especially the S-wavefield reflections, presented detailed information on the structures and physical conditions of the sediments. P-wavefield seismic sections in quick-clay environments proved useful to locate the bedrock level and layering above it, but with low resolution. However, S-wavefield seismic section presented more advantages for this geological setting presenting higher resolution images.

Keywords: Seismic methods, mineral exploration, quick-clays, seismic imaging, seismic characterization

Tatiana Pertuz, Department of Earth Sciences, Geophysics, Villav. 16, Uppsala University, SE-75236 Uppsala, Sweden.

ISSN 1651-6214
ISBN 978-91-513-1988-9
URN urn:nbn:se:uu:diva-517419 (http://urn.kb.se/resolve?urn=urn:nbn:se:uu:diva-517419)

To my family Emiro, Nidia, Felipe
and lovely partner Felix

List of Papers

This thesis is based on the following papers, which are referred to in the text by their Roman numerals.

I. **Pertuz, T.**, Malehmir, A., Brodic, B., Ding, Y., De Kunder, R., Marsden, P. (2021) Broadband seismic source data acquisition and processing to delineate iron-oxide deposits in the Blötberget mine-central Sweden. *Geophysical Prospecting*, 70(1):79–94

II. **Pertuz, T.**, Malehmir, A. (2023) Ultrahigh-resolution shear-wave reflection imaging of vertical-component data in a quick-clay prone to landslide area in southwest Sweden. *Geophysics*, 88(3):B121–B133

III. **Pertuz, T.**, Malehmir, A. (2023) Ultrahigh-resolution 9C seismic survey in a landslide prone area in southwest of Sweden. *Geophysical Journal International*, 235(3):2094–2106

Reprints were made with permission from the respective publishers.

Additionally, during my PhD studies, I have contributed to the following abstracts and papers that are not included in this thesis:

Malehmir, A., Dynesius, L., Marsden, P., Buske, S., Pacheco, N., Markovic-Juhlin, M., Brodic, B., Donoso, G., **Pertuz, T.**, De Kunder, R., Sito, L., Juhlin, C. (2020) Innovating surface and in-mine seismic exploration solutions. In *EGU General Assembly 2021*, EGU2020-11129. Abstract.

Pertuz, T., Malehmir, A., Brodic, B., Bäckström, E., Marsden, P., De Kunder, R., Bos, J. (2020) Broadband seismic data acquisition using an E-vib source for enhanced imaging of iron-oxide deposits, Sweden. In *SEG Technical Program* 2020, 81–85. Extended abstract.

Pertuz, T., Malehmir, A., Bos, J., Brodic, B., Ding, Y., Marsden, P. (2021) E-vib as an innovative seismic source in hard rock mineral exploration in

Ludvika Mines (Sweden). In *12th Annual PDAC-SEG Student Minerals.* Abstract.

Pertuz, T., Malehmir, A. (2021) Ultra-high-resolution multicomponent seismic imaging of a quick-clay landslide-prone area in southwest of Sweden. In *SEG Technical Program*, 1811–1815. Extended abstract.

Pertuz, T., Malehmir, A. (2022) 9C data acquisition for near-surface imaging in a quick-clay landslide-prone site in SW Sweden. In *Second International Meeting for Applied Geoscience & Energy*, 2128–2132. Extended abstract.

Pertuz, T., Malehmir, A. (2023) Potential of a multi-component seismic survey at a quick-clay landslide-prone area. In *Near Surface Geoscience Conference & Exhibition 2022*. Extended abstract.

Pertuz, T., Papadopoulou, M., Malehmir, A. (2023) Advances in Seismic Imaging of Quick Clays in Sweden. In *First Break*, 41(8):73–77

Contributions

The papers included in this thesis are the result of close collaborations with some colleagues and principally my supervisor A. Malehmir. My contributions in each paper are summarized below:

Paper I: I processed the seismic dataset planned and acquired by A. Malehmir in 2019. Y. Ding supported the extraction of seismic source wavelets from the E-Vib and drophammer seismic sources. The initial manuscript was written by me, T. Pertuz, and was later improved by the co-authors through a few iterations and discussions.

Paper II: I participated in the seismic data acquisition, and prepared the data and processed the 1C dataset. I wrote the initial manuscript and produced figures, which were improved after few iterations by my co-author, A. Malehmir. The work was guided under the supervision of A. Malehmir.

Paper III: I participated in the seismic acquisition, and prepared the data and processed the 9C dataset. I wrote the initial manuscript and produced figures, which were improved after few iterations with my co-author, A. Malehmir. The study was motivated and guided by my co-author A. Malehmir.

Contents

Abbreviations

2D	Two-dimensional
3D	Three-dimensional
1C	One-component
3C	Three-component
9C	Nine-component
BP	Bandpass filter
CMP	Common-midpoint
ρ	Density
DSU	Digital sensor unit
E	Young modulus
E-Vib	Electromagnetic vibrator
ERT	Electrical resistivity tomography
Ga	One-billion years (from latin *Giga-annum*)
HTI	Horizontal transverse isotropy
kyr	Thousand years
LSM	Linear synchronous motor
μ	Shear modulus
MEMS	Micro-electro-mechanical-system
NMO	Normal moveout
ORT	Orthorhombic anisotropy
pH	Potential of hydrogen
Q_p	P-wave quality factor
SPEQ	Spectral equalization filter
V_P	Compressional-wave velocity
V_S	Shear-wave velocity
VTI	Vertical transverse isotropy

1 Introduction

Sweden is in the Scandinavian peninsula, which is part of the Fennoscandian Shield. The shield is one of the crustal segments in the northwest of the East European Craton. Four orogens influenced the formation of the Fennoscandian Shield (here named from south to north, see Figure 2.1): Svecofennian or Svecokarelian orogen (2-1.8 Ga), Blekinge-Bornnhom orogen (1.5-1.4 Ga), Sveconorwegian orogen (1.1-0.9 Ga), Caledonide orogen (0.5-0.4 Ga) (Buntin et al., 2021). The study areas of this thesis, Blötberget and Lilla Edet, are in the Svecofennian (**Paper I**) and Sveconorwegian orogen (**Papers II** and **III**), respectively.

The Svecofennian orogen led to the formation of continental crust in the mainland of Sweden particularly in the north, center, and southeast. This orogeny was characterized by continuous craton collisions, leading to subduction zones with magmatic activity that led to the origin of most of the igneous rocks found in Sweden. Periods of metamorphism and intrusion of mafic dikes were marked the ending of this orogeny. Most of the iron and sulfide deposits found in the Bergslagen, Skellefte, and Norrbotten mineral districts (Bergman, 2018; Kathol et al., 2020) are believed to be the product of activities during the Svecofennian orogen. **Paper I** focuses on mineral exploration strategies in the Blötberget mine area, located in the Bergslagen region, specifically targeting the iron-oxide deposits in this region. The importance of **Paper I** is due to that Sweden has some of the richest iron-oxide mineralization in Europe (Statistics of the Swedish Mining Industry 2021, 2022). Mining activities and sustainable development goals in Sweden support advances in technology and energy transition due to the accessibility to raw materials. The demands for raw materials have steered the advancement of mineral exploration to address the necessary supply requirements. However, exploration needs to be carried out cost-effectively with a minimum environmental footprint, leading to the challenging task of identifying mineral deposits in hardrock settings.

In southwestern Sweden, the Sveconorwegian orogen reworked the western part of the Svecofennian (Bingen et al., 2005a), with continental accretion mostly developing during this orogen, resulting in a lack of metal-bearing rocks. Geological processes, such as collisions of terranes, during the Sveconorwegian orogeny at the end of the Mesoproterozoic, contributed to

high-grade gneiss complexes and low-grade metamorphic rocks in the region (Bingen et al., 2005b, 2021). Much later, during the Quaternary period, the landscape in Sweden was shaped by the latest glacial retreat and the subsequent isostatic adjustment of the underlying land mass. This changed the extent of the Baltic Sea and affected whether clays and other earth materials were deposited in marine or lacustrine environments.

Papers II and **III** highlight the importance of subsurface characterizing quick-clay areas. In southwestern Sweden, many places contain quick clays formed after the last deglaciation and post-glaciation periods. These clays are sensitive in their structure and can collapse and liquefy if their shear strength is exceeded, usually by natural or human-induced sources: this can eventually lead to the formation of landslides. Historically, quick-clay landslides in Sweden have not caused major fatalities, but caused significant economic and infrastructural losses. For instance, the largest and most known landslides in Sweden occurred in Lilla Edet in 1957, Tuve in 1977, Munkedal in 2006, and the most recent one in Stenungsund in 2023. The occurrences of these landslides have led to, first, the detection of sensitive areas prone to sliding and, second, to investigate the origin and their relation to quick-clays. Subsequently, these events highlighted the importance of characterizing soils containing quick clays. Seeing that, the motivation arose to carry out studies on soil characterization through geophysical methods with a social and economic impact.

Geophysical methods are powerful tools to investigate soils using non-invasive techniques. Seismic methods, especially used in this thesis, apply a non-destructive methodology for maximizing environmentally friendly strategies for quick-clay studies, but also providing a continuous 2D profile of the subsurface in the extremely undulating bedrock of Sweden. Following this, the papers in this thesis discuss the advantages of seismic acquisition in hardrock for mineral exploration purposes (**Paper I**) and in normally consolidated sediments with geohazard mitigation purposes (**Papers II** and **III**) where quick clays found and may lead to landslides. This thesis aims to showcase the benefits of seismic acquisition and technology innovation on two sites in Sweden: Blötberget mine (**Paper I**) and Lilla Edet (**Papers II** and **III**). The main objectives of the thesis research were:

1) Test the validity and cost-effectiveness of a vertical-type electromagnetic vibrator (E-Vib) as a seismic source for hardrock settings (**Paper I**),
2) Delineate iron-oxide deposits at the Blötberget mine using broadband seismic data from the E-Vib and using a tailored processing workflow (**Paper I**),

3) Retrieve the S-wave reflection from a vertical-impact source recorded on vertical-component geophones in a quick-clay setting in southwestern Sweden (**Paper II**),
4) Image the P-P and S-S wavefield reflections from a 9C dataset in the same study area as the latter study (**Paper III**),
5) Provide insight on the benefit of 9C seismic data acquisition for quick-clay landslide studies (**Paper III**).

Paper I was developed under the Smart Exploration™ project, sponsored by the European Commission through an H2020 (Horizon 2020 programme) grant. The project allowed development of new prototypes and solutions, and investigation on innovative geophysical solutions for mineral exploration, from prototypes to how-to as documented by several works e.g., Hloušek et al., (2022), Malehmir et al. (2017), Maries et al. (2017) and (2020), Markovic et al. (2019 and 2020), among others.

1.1 Thesis outline

This thesis is structured by seven chapters and three papers as an outcome of my PhD studies. *Chapter 1* introduces the research topic and main objectives. *Chapter 2* presents the study areas, including a geological description, earlier studies, and the rock physical properties. *Chapter 3* provides the theoretical background necessary to follow the research work. *Chapter 4* includes topics that were out of the thesis scope, but highlight the importance of future research. *Chapter 5* summarizes the three papers produced during the PhD studies. Conclusions are given in *Chapter 6* and afterwards a summary of the thesis is provided in Swedish and Spanish.

This thesis includes three published papers developed in two study areas. **Paper I** focuses on a compressional-wave seismic dataset from the Blötberget mine in Sweden, where an electromagnetic vibrator (E-Vib) was tested for the first time in hardrock for mineral exploration purposes. Results were compared with previous seismic studies along the same profile using a 500-kg drophammer seismic source. During the comparison, the advantages on the E-Vib seismic data are discussed compared to the earlier surveys.

Papers II and **III** involve datasets from Lilla Edet, in southwestern Sweden, using 1C and 9C data acquisition. **Paper II** shows the results of an ultra-high-resolution dataset where shear-wave reflections were retrieved from the 1C-geophones. The datasets helped to image in detail the subsurface sediments and bedrock complexity. **Paper III** exhibits the advantages of 9C data acquisition in the same site as **Paper II**. This dataset shows its richness and reveals

wavefield complexity that helps to extract information such as anisotropy parameters.

Overall, this thesis work exploits the possibility of using new types of seismic sources for hardrock mineral exploration applications; opening up the opportunity to include tailored processing workflows to maintain the source signature and comparing it with previous acquisitions to highlight its benefits. In addition, seismic methods are also presented that have applicability in normally consolidated sediments in hazardous areas in Sweden. This thesis therefore helps in better understanding how quick clays can be characterized using seismic methods, a step forward in developing geophysical methods for geohazard studies.

2 Case studies

2.1 Blötberget

Blötberget is situated in the Ludvika Municipality (**Paper I**) in central Sweden, and in the historical mineral district of Bergslagen (Figure 2.1). Bergslagen is a mineral-endowed region and has played a significant role in the Swedish economy because of its iron ore production for over 800 years (Stephens et al., 2009). Minerals from Bergslagen have supported the economic growth and development in Sweden. They have paved the way for industrial innovation such as the invention of three-phase electricity transmission and drilling and mining equipment. Recently, improved iron ore prices and the presence of high-quality iron oxide deposits have motivated Nordic Iron Ore (NIO) to reassess these deposits in Blötberget. This improves resource estimation and exploration and is a step forward for a renewed mining operation in the region. The complex host rock structure and the challenging geological setting required several geophysical studies and allowed an extensive set of seismic surveys to be acquired, as well as testing of new technologies in the area (Malehmir et al., 2020).

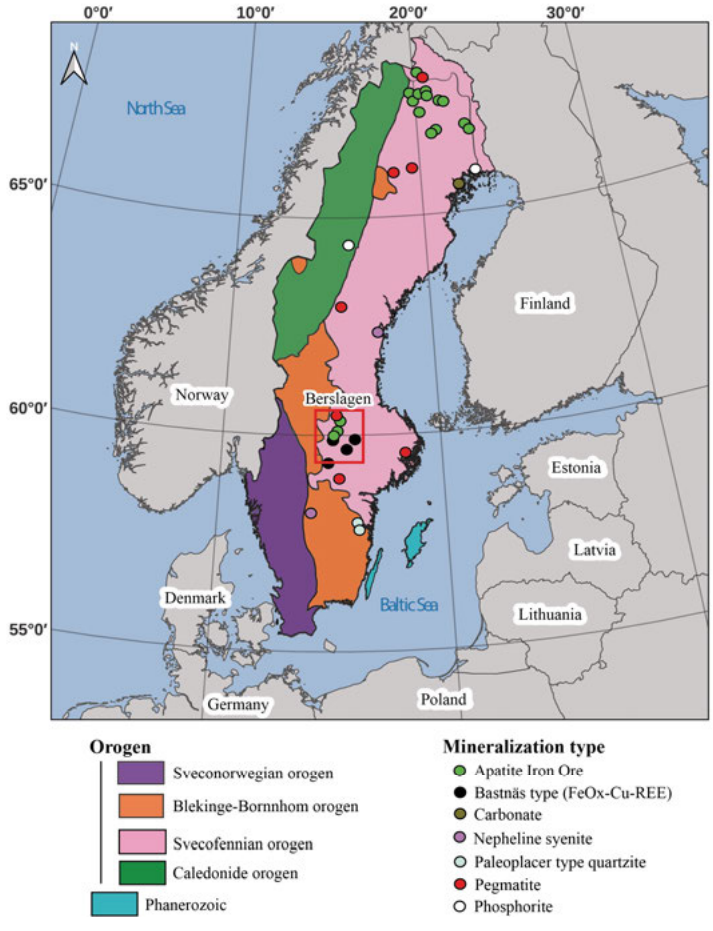

Figure 2.1. Simplified geological map of Sweden is shown with key critical raw material occurrences in the Bergslagen district (adapted from Buntin et al., 2021 and Sadeghi et al., 2013). The blue region corresponds to sedimentary rocks from the Phanerozoic. The red rectangle is the focus of **Paper I** in the Ludvika mining area.

2.1.1 Geology of Blötberget

Blötberget mine, in the Bergslagen district, is in the Fennoscandian Shield, dominated by metamorphosed volcano-sedimentary rocks of Paleoproterozoic age (1.91-1.87 Ga). The Svecofennian orogen deformed the region leading to metamorphism in rocks and complex folding structures. The Ludvika region shows a characteristic fold with northeast-southwest strike as an aftermath of the orogenic process (Stephens et al., 2009). Profitable parts of the iron oxide deposit are mainly in sheet-like layers within inliers of feldspar and

porphyritic meta-volcanic rocks. Pegmatite and mafic dykes are observed crosscutting the host rocks and mineralization (Markovic et al., 2020).

2.1.2 Mineral resources

Sweden is a leading mineral producer within the European Union. Ore production recently reached approximately 88.6 million tonnes and it has increased by 22% in the past years (SGU, 2023) with iron ore being the dominant. Historically, most of the iron produced in Sweden came from Bergslagen (Stephens et al., 2009), however, Norrbotten and Kiruna are today leading producers of iron ore in Sweden and Europe.

The Blötberget mine and the Ludvika region in general have been the center of several geological and geophysical surveys since the 1950s to gain knowledge on the depth and lateral extent of these iron-oxide deposits. Shallow deposits were discovered using magnetic-based methods, and these deposits were exploited until their economic conjuncture in the late 70s. In 2011, iron ore prices increased, and with them mineral exploration. Blötberget resources are estimated to be c. 45.4 million tons of measured and 9.6 million tons as indicated, with an average of 41.7% and 36.2% of iron respectively (Nordic Iron Ore, 2017). Blötberget mineralization occurs in four sheet-like horizons. They contain approximately 40% magnetite and hematite and some zones have more magnetite than others (Nordic Iron Ore, 2017).

2.1.3 Previous seismic studies

Previous seismic studies helped to characterize their physical properties and suggest a depth extension of the deposits (Malehmir et al., 2017; Maries et al., 2017; Almqvist et al., 2019). Gravity and magnetic surveys in 2015 provided an improved gravity map, reported by Yehuwalashet and Malehmir (2018), which identified the location of known mineralization and potential regions for further mineral exploration. In 2016, a geophysical campaign worked towards imaging the mineralization and its depth extension using conventional seismic methods (Malehmir et al., 2017; Bräunig et al., 2019; Balestrini et al., 2020; Maries et al., 2020; Markovic et al., 2020; Malehmir et al., 2020). Maries et al. (2017) focused on studying the host structures, fracture zones, and depth extent of the mineralization, which was suggested to extend down to 1200 m depth. Downhole logging data in seven boreholes were also acquired and reported on by Maries et al. (2017).

Complementary works in combination with borehole data also suggest the presence of a deeper mineralization and a crosscutting reflection, which may truncate deeper parts of the mineralization (Maries et al., 2020; Markovic et

al., 2020). Given the probability of the existence of new deposits and to properly account for 3D effects and structures, a sparse 3D seismic survey was acquired and further indicated a lateral extension of 300 m towards the west and a fault system at the termination of the deposits (Malehmir et al., 2021). All these studies were successful in illustrating the use of seismic methods for mineral exploration and showed that the site is favorable for testing deep exploration technologies including the use of broadband seismic sources that are part of this thesis work.

2.1.4 Physical properties

The study of physical properties in Blötberget was based on seven boreholes downhole logged in the area. Magnetic susceptibility and natural gamma radiation were measured in all seven boreholes. Formation resistivity, fluid temperature, fluid conductivity, and triple sonic full-waveform logging were done in boreholes where conditions were good and the diameter was wide enough for these probes (Maries et al., 2017). Iron-oxide deposits, especially magnetite, are identifiable from their magnetic susceptibility. Figure 2.2 shows the magnetic susceptibility of the boreholes from NW to SE, highlighting a SE-dipping direction of the mineralization. Peaks in the natural gamma log indicate the richness of K-feldspar minerals, which are not present in the mineralization, but in pegmatites which are intersected. Maries et al. (2017) further provided information on the rock quality based on the seismic quality factor calculated from the triple sonic data. Low Q_P values were observed in the mineralization zones, implying poorer competent materials than their host rocks. From the synthetic seismograms in Maries et al. (2017), it was suggested that the mineralization should be strongly reflective. In conclusion, elastic properties indicated a strong contrast between the magnetite and hematite-bearing zones with their host rocks, justifying why seismic methods could be used in the area.

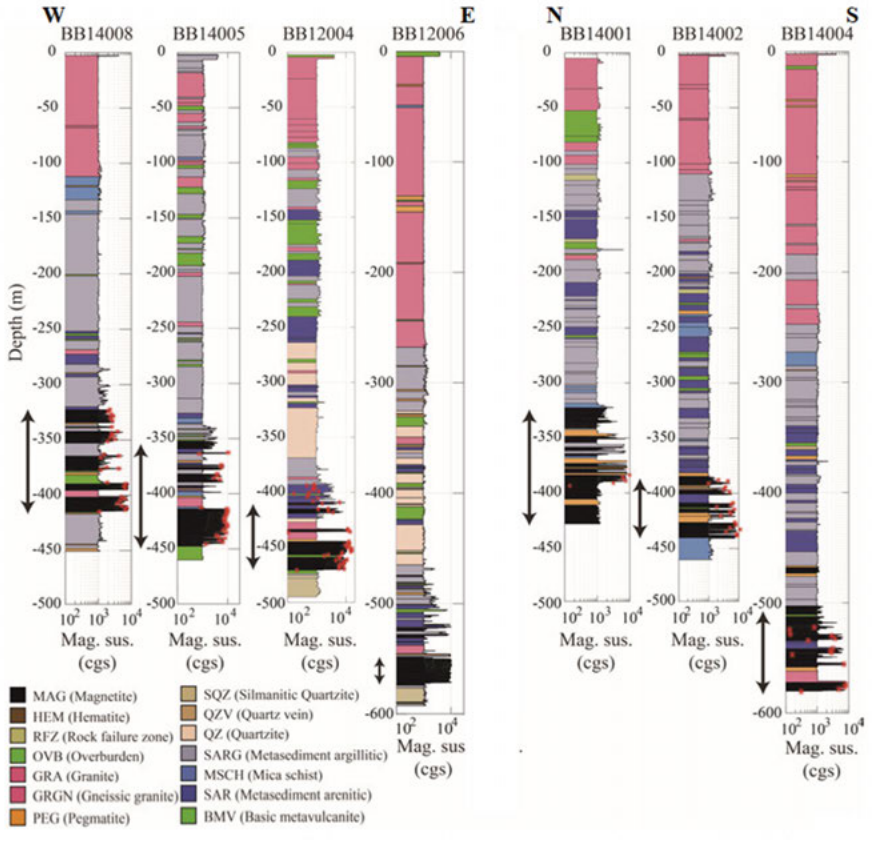

Figure 2.2. Magnetic susceptibility downhole logged in different boreholes in the Blötberget mining area. Red stars show laboratory measurements in zones of high magnetite content (Maries et al., 2017).

2.2 Lilla Edet

Lilla Edet, the subject area of **Papers II** and **III**, is situated in the Götaälv zone in the southwestern Sweden (Figure 2.3a). The Göta River is the largest river in Sweden and supplies fresh water for the region; it flows from Lake Vänern to Gothenburg city, the second largest city in Sweden. Therefore, important industries, power stations, dams, and other infrastructure are located along and adjacent to the river. However, this area is characterized by a high frequency of landslides (Report SGI, 2012), historical ones and local ones, indicated by the presence of multiple scars along the river shores (Figure 2.3a). Lilla Edet itself has a record of a historical landslide in 1957, known as the Göta slide, and caused an environmental catastrophe because of the displacement of chemical materials into the river.

2.2.1 Geology

Geological characteristics and landscapes in Sweden are shaped by glaciation periods starting in the Pleistocene (De Geer, 1940) and continuing until 10-11 kyr ago. Rivers (e.g., the Göta River) were formed in weak zones as the glaciers aggressively carved out bedrock along fault and fracture zones. Göta River drains fresh water from Lake Vänern towards the south, acting as a medium of transportation for sediments. It deposited layers of clays along the shoreline in the last deglaciation (Figure 2.3b). Therefore, glacial, and post-glacial sediments were deposited in a marine environment. These are now uplifting (due to the post-glacial rebound, and isostatic adjustment, of the lithosphere) forcing freshwater infiltrations into the sediments formed in marine or brackish waters. This means a continuous process of leaching clays from their salt content (either in their pores or as solid salt). While still a matter of debate, it is unclear if freshwater infiltrates vertically through the clays or takes a path via bedrock and interbedded permeable layers (silty-sandy layers), leading to the formation of quick clays (Osterman, 1963; Torrance, 2012). If clays are vertically leached, quick clays should be found from top-down, however, at some sites, quick clays are found above coarse-grained materials (or sometimes referred to as “friction layer”) implying these materials act as a conduit or confined aquifer for freshwater, literally leaching overlying clays (Malehmir et al., 2013a) and forming quick clays from bottom-up. Generally, quick clays should meet specific stratigraphic and geohydrological requirements to lead to the development of the “quickness” property (summarized by Salas-Romero et al., 2019; and extensively reviewed by Rankka et al., 2004). Stratigraphically, clay deposits should be interbedded by permeable layers, such as coarse-grained materials, and deposited over a complex and undulating bedrock. On the geohydrological side, the presence of artesian groundwater pressure, organic soils, and infiltration involving several directions influence the formation and triggering of a quick-clay landslide.

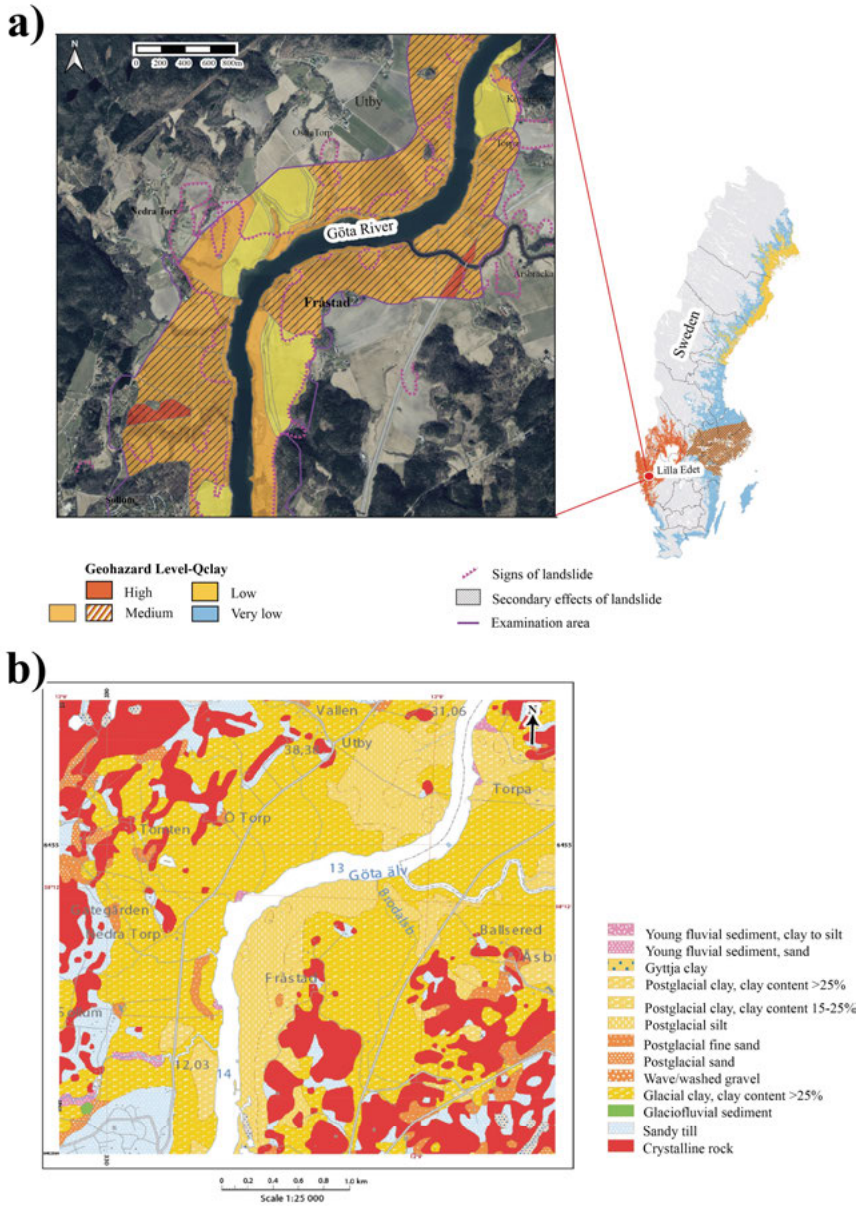

Figure 2.3. (a) Outset showing the landslide risk map of Sweden and the location of the study area (**Papers II** and **III).** (b) Surface geological map indicating a predominance in glacial and post-glacial clays in the Göta River area. Maps are modified from SGU's website.

2.2.2 Quick or sensitive clays

Quick or sensitive clays form consolidated bodies (solid) in undisturbed condition will liquefy when remoulded, meaning they lose their shear strength when disturbed or exposed to excess pore-water pressure as illustrated in Figure 2.4b and c (Bjerrum and Rosenqvist, 1956; Osterman, 1963; Söderblom, 1963; Rosenqvist, 1966; Appelo and Postma, 2004; Rankka et al., 2004; Khaldoun et al., 2009). Quick-clays typically have high water content, meaning that when seismic studies are conducted, P-wave velocities are typically around 1400-1500 m/s while shear-wave velocities are distinctly slower, usually about 60-150 m/s (or there is sometimes no or only little shear strength). Mineralogically, quick-clay deposits consist of mainly non-swelling clay minerals, which have water limits lower than their intrinsic water content (Rankka et al., 2004; Mitchell et al., 2005).

Clay sensitivity is a property that identifies whether the deposit can reach its quickness behavior, defined by the ratio of undisturbed to the remoulded shear strength of the soil (Lefebvre, 1996). It is also influenced by factors such as pH levels, dispersing agents, and external mechanical forces (Bjerrum and Rosenqvist, 1956; Talme et al., 1966; Fällman et al., 2001; Mitchell et al., 2005). Those inherent conditions determine the clay sensitivity property, thus its shear strength, which if external forces (e.g., constructions, river erosion, earthquakes) overload them, then the clays become quick or liquefy (Torrance, 2012; Tran et al., 2017; Salas-Romero et al., 2019).

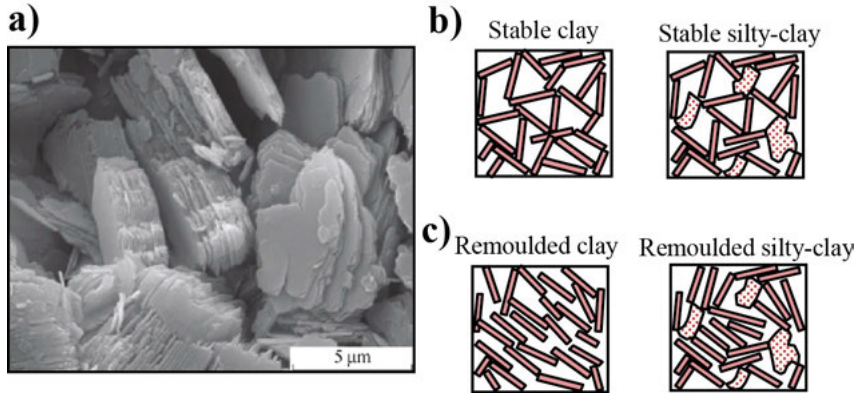

Figure 2.4. (a) Scanning electron microscope picture of one of the most common clay-types: Kaolinite, reflects the flat, sheet-like and tetrahedral shape of clay (Savko et al., 2019). When a clay or silty clay is (b) stable its sediments form a 'house of cards' shape (many contact points) but if it liquefies (c) the cards collapse leading to unstable or collapsed sediments.

2.2.3 Previous site investigations

Geophysical and geotechnical studies were conducted in 2011, 2013 and 2020, and focused on obtaining knowledge on quick clays, their host stratigraphy and their formation at the study area (e.g., Malehmir et al., 2013a, b; Shan et al., 2014). Gravity and magnetic surveys provided bedrock topographical information that was later confirmed by seismic methods. Electromagnetic methods, controlled-source and radio-magnetotellurics, provided useful information, but to only a limited depth because of the high conductivity of the marine clays (Malehmir et al., 2013a). In the case of ERT, a depth of 30 m was reached identifying intermediate layers, but not the bedrock and its complex morphology (Malehmir et al., 2013a).

Seismic methods successfully provided higher resolution data and detailed images of the subsurface; they were attempted in a wide range of 2D and 3D configurations in the study area (Malehmir et al., 2013a; Lundberg et al., 2014; Salas-Romero et al., 2019). Lundberg et al. (2014) studied a 3D dataset over a landslide scar in the study area. Salas-Romero et al. (2016) determined physical and physicochemical properties through downhole logging to recognize the geological conditions of the quick clays in the area and their relationship with the coarse-grained layers underneath them. The northern side of the landslide scar was characterized by Salas-Romero et al. (2019). The authors proposed a hydrological model using results from the seismic and borehole data and explained the hydrogeology of the site when compared to water levels observed in wells available in the study area. Meanwhile, the results from the 2011 P-P and SH-SH wavefield surveys justified the importance of further research in the region using more dedicated seismic investigations. To improve the results from the 2011 acquisition, where a 2-4 m source and receiver spacing was used (Malehmir et al., 2013a, b; Salas-Romero et al., 2016; Krawczyk and Polom, 2018; Salas-Romero et al., 2019), in 2020, a new seismic survey was performed employing 1 m source and receiver spacing to ensure a less aliased shear-wave retrieval from the dataset. This was a limiting factor in the 2011 data as addressed by Malehmir (2019 and 2020) when an attempt was done to retrieve shear-wave reflections from the 2011 vertical component seismic data.

2.2.4 Downhole and borehole physical properties measurements

A wealth of different data is available from the study area, including cone penetration tests with resistivity (CPTU-R), borehole logging and sampling measurements in three boreholes reported by Löfroth et al. (2011) and Salas-Romero et al. (2016), respectively. The borehole BH1 is the only one that

crosses the studied profile and it is located in the center of it. Therefore, logging measurements of only BH1 are described here. The CPTU-R works indicated low resistivity above bedrock meaning saline clays and potential quick clays above the coarse-grained layers on the western side of the study area. During the drilling operations, the fluid temperature suggested an in-situ groundwater gradient at shallow levels in BH1. Borehole logs shown in Figure 2.5 correspond to BH1, which is located on profile 1 (used for studies in **Papers II** and **III**), and include near- and far-waveforms, natural gamma, and magnetic susceptibility (Mag. Suscep.) logs. Velocity sonic measurements were limited by the PVC casing in the borehole; therefore, only the section with a perforated PVC casing could be logged and yielded an average P-wave velocity (V_p). Gamma Ray logs provided information on the soil column, suggesting predominantly clay and silty clay with sandy-silt alternations. For instance, natural gamma ray measurements increase from clay to coarse-grained materials, while the magnetic susceptibility increases in sandy-silty materials. Electrical conductivity measurements, reported by Salas-Romero et al. (2016), suggest salinity increases with depth, as is common on clayey sediments deposited in marine to brackish environments.

From the laboratory measurements, analysis of exposed outcrops, and cross plots, Salas-Romero et al. (2016) suggested two magnetic materials predominant in the area. One corresponded to the coarse-grained layer with low magnetic mineral concentration and high coercivity, or paramagnetic, identified as titanomagnetite in fluvial sediments, explaining the change on the magnetic susceptibility logs. Another mineral called titanohematite with a ferromagnetic property is found in bedrock outcrops. These strong responses from the coarse-grained layer and the bedrock facilitated the identification of their layers at different borehole depths.

BH1 shows that fine clays are the predominant fraction observed along the borehole with salinity values <2 g/l on the first 22 m and last 6 m of the borehole of the 36 m deep borehole (Salas-Romero et al., 2016), indicating clay leaching at those depth points (Torrance, 1974; Salas-Romero et al., 2016). In terms of flocculation processes, low pH values were detected at shallow depths and under the coarse-grain layer, meaning probable quick clays within the sediments (Torrance and Pirnat, 1984).

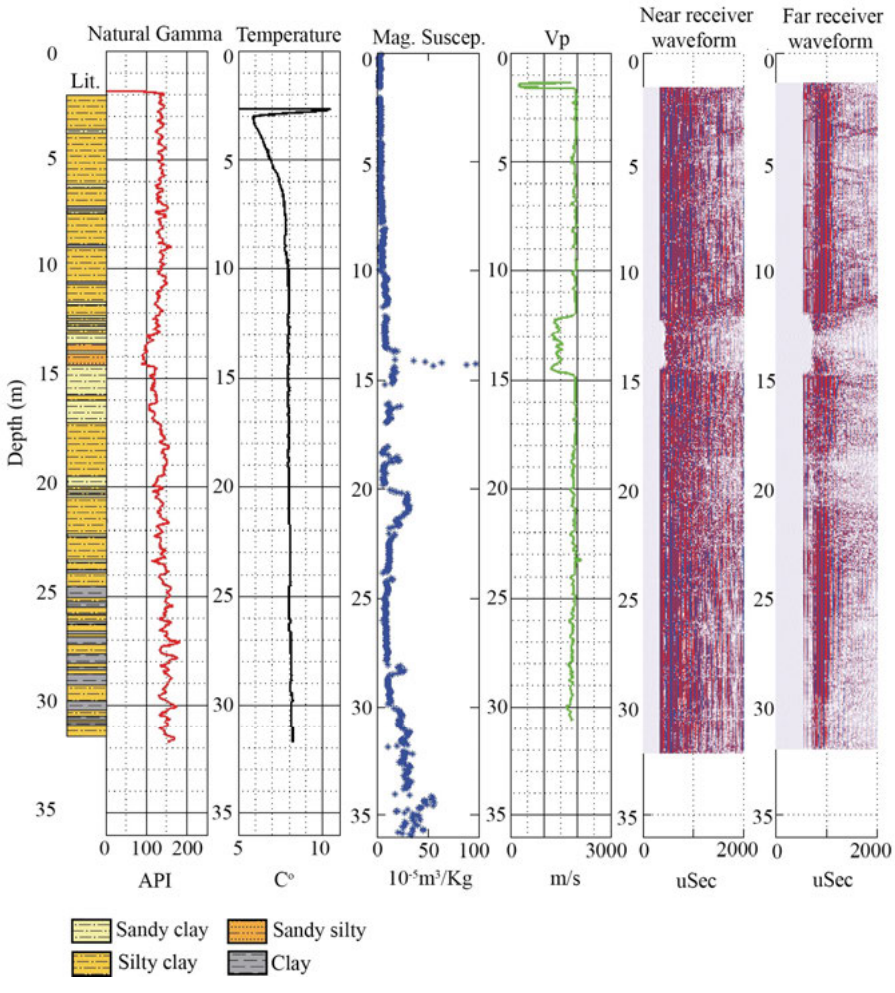

Figure 2.5. Borehole logging and physical properties measurements from BH1 on Profile 1 (the focus of **Papers II** and **III)**. Lithology (Lit.) interpreted from the Natural Gamma ray log, Natural Gamma ray, fluid temperature, magnetic susceptibility (Mag. Suscep.), P-wave velocity (V_P), and near and far receiver waveforms are shown in different panels, respectively. Soil texture was obtained from the combined measurements and analysis. (A. Malehmir, personal communication, 2023)

3 Seismic wavefield and data acquisition

Seismic wavefield studies allow temporal and spatial knowledge of the media to be obtained. Each wave-mode provides different information about the rock and its fluid content because of the particle polarization during the propagation of a seismic wave. Given the nature of various wave-modes, symmetry planes of the propagation media can be illuminated allowing the estimation of its physical properties e.g., elastic constants, anisotropy axes, fluids, and lateral heterogeneities. This highlights the importance of fundamental seismic studies, not only on a scalar-base, but also a vector-base, thus, introducing the need of understanding and interpreting the direction of earth displacement.

3.1 Wavefield complexity and richness

In a homogenous media, three wave-modes propagate independently, a compressional or P-wave and two shear waves or SV and SH waves (Figure 3.1). The particle motion generated by a propagating P-wavefield, or compressional wave, is in the same direction as the propagation-vector, while the particle motion generated by the SV-wavefield is perpendicular to this. When a P-wavefield encounters an interface with sufficient elastic property contrasts, then it may reflect and transmit SV-wave-modes (Yilmaz, 2001). SH-wavefield propagation is like SV-wavefield but its particle motion occurs on an opposing horizontal plane and is decoupled from the P- and SV-wavefields.

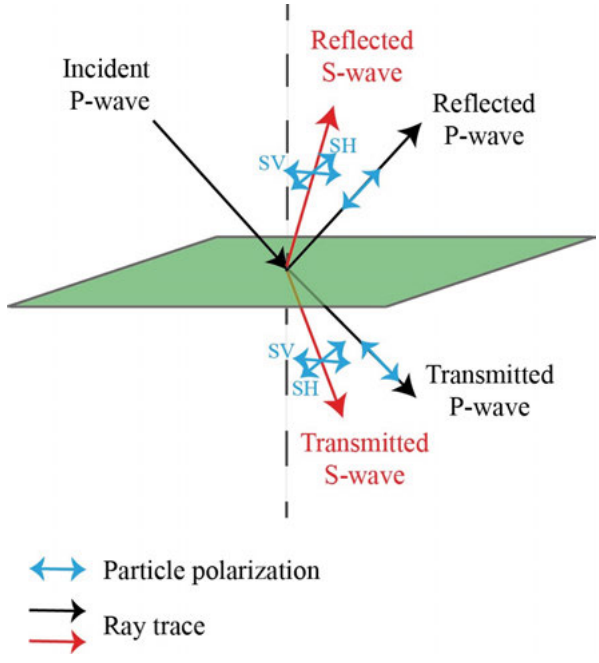

Figure 3.1. Ray diagram of different wavefields traveling through an interface. Incident P-wave can produce a reflected and transmitted P- and S-wave (solid black and red arrow, respectively) when it interacts with an interface. Each wave is characterized by a different direction of the particle motion as shown, depending on the wave-type, in blue arrows. Adapted from Hardage et al. (2011).

Wavefield propagation is dependent on the elastic properties of the medium. The elastic properties can be described by elastic constants, such as bulk modulus, shear modulus, Poisson ratio, etc., which affect the particle motion as the wave propagates. P-waves propagate in a compressional and extensional manner through the materials resulting in a temporal change of (very negligible) volume while it propagates through. This is described by the bulk modulus, K, which indicates the resistance of a rock when uniform pressure is applied in all directions and its inverse gives the rock compressibility (Figure 3.2a). The SV-wave-mode, instead, results in a change of shape, distorting the volume in the x- and z-directions. The shear modulus, μ, provides the rock rigidity when shear forces are exerted per unit area (Figure 3.2b). These elastic constants are expressed by the following equations in relation to the corresponding wave velocity and density (ρ):

$$V_P^2 = \frac{K+\frac{4}{3}\mu}{\rho} \text{ and } V_S^2 = \frac{\mu}{\rho} \tag{3.1}$$

The relation of P- and S-wave velocities is given by the Poisson's ratio (assuming an isotropic medium), *v*, which relates the deformation of the rock perpendicular to the direction of the applied forces (Figure 3.2c):

$$v = \frac{\frac{V_P{}^2}{V_S} - 2}{2\left[\frac{V_P{}^2}{V_S} - 1\right]} \tag{3.2}$$

The Young's modulus (*E*) provides information on how easily materials stretch and deform, and thus, relates the axial stress (σ) to the axial strain (ε) along the same direction through $E = \sigma / \varepsilon$, (Figure 3.2d). These elastic constants characterize the medium that the waves propagate in.

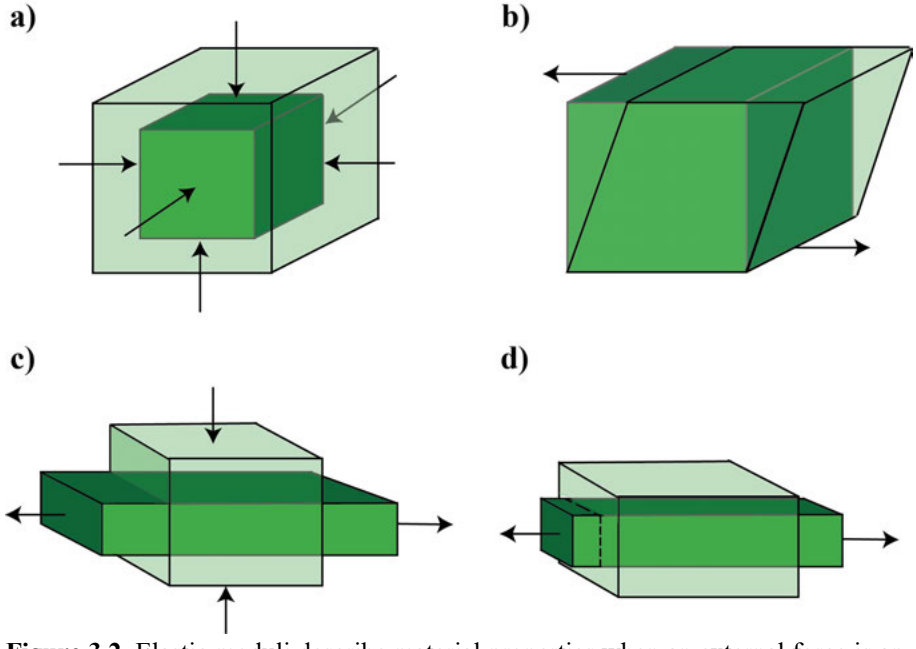

Figure 3.2. Elastic moduli describe material properties when an external force is applied (black arrow). The main elastic moduli classified by the direction of the applied force are (a) Bulk modulus, (b) Shear modulus, (c) Poisson's ratio, and (d) Young's modulus (not independent of bulk and shear moduli). Modified from Healy et al. (2020).

Since the Earth is not homogenous and can even be anisotropic, each wavefield senses different information and varies as a function of direction. Nevertheless, a symmetry classification as vertical transverse isotropy (VTI), horizontal transverse isotropy (HTI), and orthorhombic media (ORT) can characterize medium heterogeneity, which can be from grain size, thin layering, or due to thick stratigraphic sequences (Fjær et al., 1996). VTI involves a vertical

symmetry axis perpendicular to the layers with no lateral variation (Figure 3.3a). This type of medium can represent clays and shales. If the symmetry plane is horizontal (Figure 3.3b), where vertical layers are uniform, then it is considered an HTI medium. This anisotropy type is usually associated with cracks and fractures. Another anisotropy case is the orthorhombic media (ORT), which includes two orthogonal planes. One of the planes is parallel to the stratification layers and the other one is perpendicular to this plane. This perpendicular plane can be a set of main fractures oriented along the plane (Figure 3.3c).

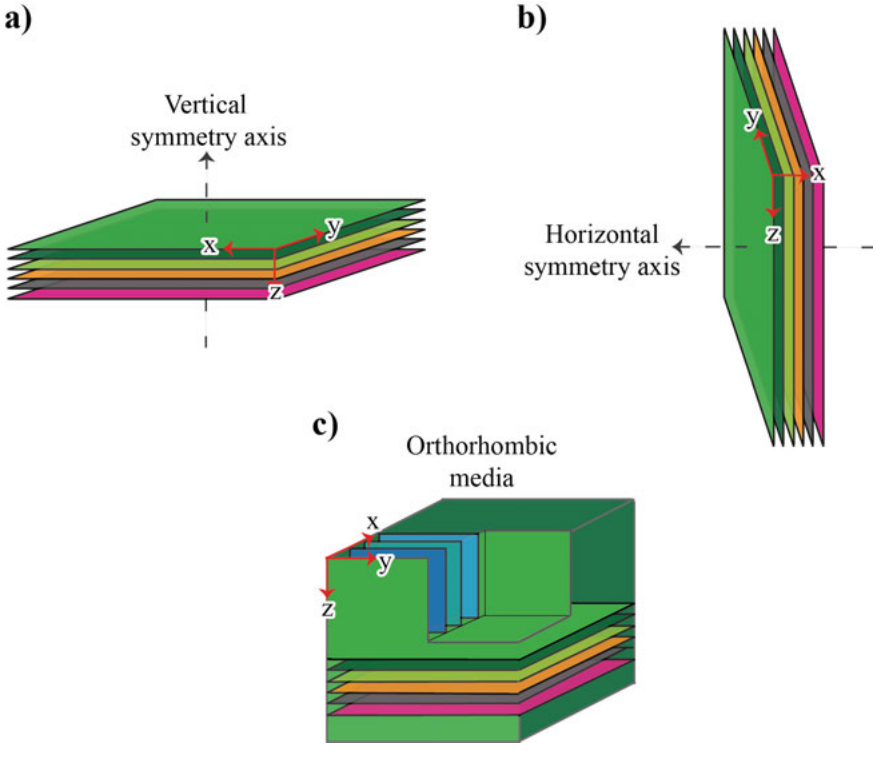

Figure 3.3. Anisotropy classification according to the symmetry of heterogeneities. (a) Vertical Transverse Isotropy (VTI). (b) Horizontal Transverse Isotropy (HTI). (c) Orthorhombic symmetry (ORT).

3.1.1 Radiation pattern

Wavefield radiation patterns are polar plots that represent the amplitude of a component with respect to applied forces (Figure 3.4). This diagram represents the wavefield amplitude variation at different take-off angles. The P-

wave radiation, U_P, when a vertical source-direction is applied on a free surface in a half-space, is described by (Gaiser, 2016):

$$U_P \sim \frac{\cos\theta\left(\gamma^2 - 2\sin^2\theta\right)}{F_0(\sin\theta)} \tag{3.3}$$

Where θ is the vertical angle, $\gamma = V_P/V_S$ and F_0 is:

$$F_0(\zeta) = (2\zeta^2 - \gamma^2)^2 - 4\zeta^2\sqrt{(\zeta^2 - 1)(\zeta^2 - \gamma^2)} \tag{3.4}$$

Where $\zeta = sin\theta$. SV-wave radiation produced by a vertical source-direction follows the variation:

$$U_{SV} \sim \sqrt{\gamma^5}\,\frac{\sin 2\theta\sqrt{\gamma^2\sin^2\theta - 1}}{F_0(\gamma\sin\theta)} \tag{3.5}$$

One characteristic to highlight between P- and SV-displacement is that the P-wave phase response is the same for all propagation angles, but SV has a polarity reversal at θ=0° and its energy is proportional to the distance (Gaiser, 2016).

Horizontal source-direction can produce all types of wave-modes, i.e., P, SV, and SH. Miller et al. (1954) developed an expression for SV- ($U_{SV}^{(x)}$) and P-wave ($U_P^{(x)}$) radiation pattern produced by a horizontal force:

$$U_{SV}^{(x)} \sim \sqrt{\gamma^7}\,\frac{\cos\theta\cos 2\theta}{F_0(\gamma\sin\theta)} \tag{3.6}$$

$$U_P^{(x)} \sim \frac{\sin 2\theta\left(\sqrt{\gamma^2 - \sin^2\theta}\right)}{F_0(\sin\theta)} \tag{3.7}$$

Strong SH-waves are generated and recorded in the orthogonal plane. The strength is described by (Cherry, 1962):

$$U_{SH}^{(x)} \sim \sqrt{1/\gamma}\,(\sin\emptyset) \tag{3.8}$$

where $\emptyset$ is the azimuth. Figure 3.4a shows the radiation pattern for P- and SV-wavefields produced by a vertical displacement force in a 3D plot. It shows that SV-wave strength (U_{SV}) is larger than P-wave (U_P), a factor highly dependent on the V_P/V_S ratio. Figure 3.4b depicts the radiation pattern of

different waves when using a horizontal displacement point force, where $U_{SV}^{(x)}$ is propagated strongly and $U_P^{(x)}$ has a small amplitude. In the case of $U_{SH}^{(x)}$, it can be only produced by an SH source, and in this case its wave propagation is steady and strong. It is worth mentioning the effect of V_P/V_S on wave propagation. Figure 3.4 is a typical case of a high V_P/V_S ratio while for a low ratio the energy for S-wave is consumed by the P-wave radiation.

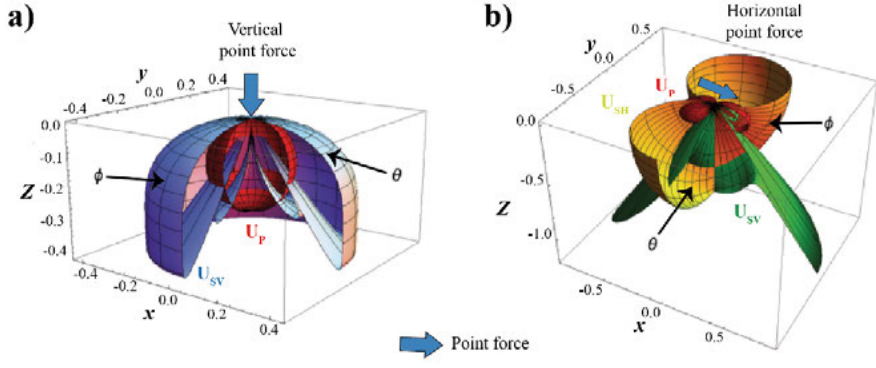

Figure 3.4. 3D radiation pattern plots for P- (U_P), SV- (U_{SV}), and SH-waves (U_{SH}) originated by (a) vertical and (b) horizontal sources. The color scale for the plots is dependent on the x-component. Modified from Gaiser (2016).

3.1.2 Wave-mode conversion

Wave-mode conversion occurs when the energy propagated in a medium is partitioned at an interface. The importance of the wave-modes is that each of them senses different properties of the materials. Various wave-modes are recorded according to the type of equipment and seismic data studied. One-component (1C) data consists of 1C receivers and a unidirectional source that will usually capture a P-P mode. Three-component (3C) data are acquired when using 3C receivers and a one-component source to illuminate different wave-modes. These modes are dependent on the source orientation. A nine-component (9C) dataset is the result of the coverage of three orthogonal sources and receiver-vectors at the same recording point. This will capture all possible wave-modes: P-P, P-SV, SV-SV, SV-P, SH-SH. The notation for the modes relates the downgoing-upgoing wavefield, separated by a hyphen. Worth noting, SV- and P-modes are coupled during reflection, but SH does not have energy exchange with any other wave-modes.

Surface waves, i.e., Rayleigh and Love waves propagate near the surface and are recorded by the sensors. Rayleigh waves are combinations of P- and SV-wave motions, while Love waves are formed by the constructive interference

of multiple reflected SH-waves at the near surface. The motion of the Rayleigh wave is elliptical in the radial and vertical plane, and Love wave motion is linear in the transverse direction. As different wave types have their particle motions in different directions (i.e., polarized in different directions) their polarizations can be examined in a coordinate system which is directed from the source to the receiver. In this case the source-receiver direction will be the radial component/direction, and the transverse component/direction will be in the horizontal plane, perpendicular to the radial one.

For anisotropic media, where material properties differ according to different directions, a special wave-mode needs to be considered; as shear-wave splitting may occur (Figure 3.5): fast-S (S_1) and slow-S (S_2). The names of these wave modes are given by their difference in the velocities. The particle motion of the fast-S (S_1) is usually oriented parallel to the "bedding", while the slow-S (S_2) particle motion is perpendicular to it, but travels along the same direction as the incident S-wavefield. Therefore, S_1 will propagate further than S_2 in a given time. In terms of polarization, the preferred direction of S_1 will be the maximum stress orientation and S_2 towards the minimum stress. Worth noting, that the larger the time difference between the S_1 and S_2 traveltimes, the larger the anisotropy.

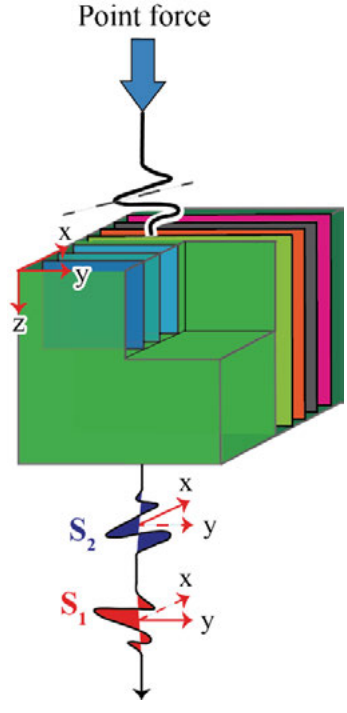

Figure 3.5. Illustration of a seismic wave propagating through an anisotropic medium. As a product, shear-wave-modes are classified because of the difference in velocities as fast-S (S_1) and slow-S (S_2). Both modes travel in the same direction, but their particle polarization is orientated along and perpendicular to the symmetry axis. Adapted from Hardage et al. (2011).

3.2 Multicomponent data acquisition

In this section, different seismic receivers and sources used during the data acquisition of **Papers I**, **II**, and **III** are described.

3.2.1 Seismic receivers

A seismic receiver is a device that measures ground perturbations and converts them into electrical signals and according to the acquisition aim this can be geophones, accelerometers, hydrophones (for offshore acquisition and not used in this study), distributed acoustic sensing (DAS, not used in this study) or piezoelectric (often used in the laboratory, but has come into the receiver-domain industry). Geophones measure particle velocity and record analog signals that need to be digitized (Hardage et al., 2011). A geophone consists of a magnetic coil hanging from a spring and a metallic spike that connects to the ground (Figure 3.6a). Geophones are classified in 1C, typically referred to as vertical, and used in **Papers I** and **II**, but also 1C-horizontal for reflection and refraction seismic, and 3C or multicomponent for advanced soil studies (Hardage et al., 2011). The recorded frequency band in seismic receivers is bounded by their natural frequency, the minimum frequency given by the resonance frequency of the geophone mass, and the spurious frequency, the maximum frequency recorded by the geophone (Maxwell, 2014).

A type of 3C sensor, used in **Papers II and III**, is a MEMS-based (micro-electro mechanical system) sensor, which is a digital sensor that records particle acceleration. Like geophones, MEMS measure the inner hanging mass displacement (Figure 3.6b), which values are digitized internally to, usually, what a geophone can maximally record in terms of voltage. This sensor is more useful because its design allows a steady signal recovery, hence no attenuation (Hons et al., 2008). Given the broad frequency bandwidth, ranging from 0-800 Hz, higher frequencies can be better detected than a normal geophone. MEMS are accelerometers; hence, they measure gravitational changes (usually to a maximum of 0.5g).

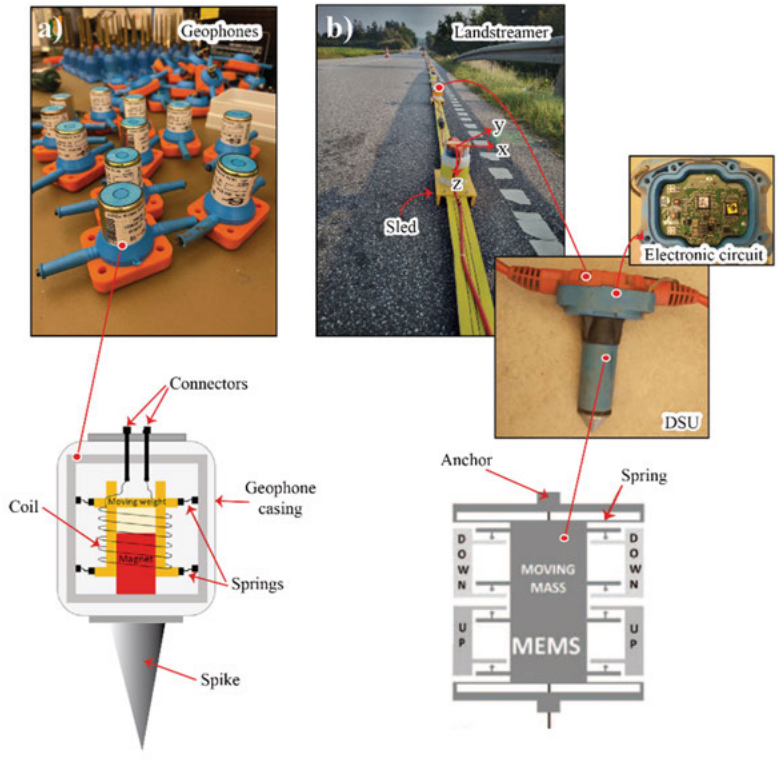

Figure 3.6. Different types of seismic receivers are used for the seismic data acquisition in this thesis work. (a) 1C vertical geophones typically work when the magnet movement within the coil is actioned by the transmitted seismic wave, which travels along the buried spike. Modified from Guideline Geo (www.guidelinegeo.com). (b) 3C MEMS-based sensor, in a landstreamer array, is mounted on a sled to be used on roads. The digital sensor unit (DSU) consists of internal electronic components. Adapted from Laine and Mougenot (2014).

3.2.2 Types of seismic sources

Seismic sources are important in active seismic acquisition because they should be able to generate sufficient energy to penetrate the earth layers without much source-generated noise amplifications. Land seismic sources can be impulsive and non-impulsive. Impulsive sources, such as sledgehammers, weight-drops, explosives, etc., require generating an energetic wave of short duration into the ground. Sledgehammers (Figure 3.7a) are commonly employed, especially in small-scale acquisition settings for near-surface targets; used in **Papers II** and **III**. The sledgehammer is used by hitting a metallic plate fixed on the ground to generate different seismic waves in different vertical and horizontal orientations as described in **Paper III**.

Non-impulsive sources, for instance, vibrators, transmit energy to the ground for longer periods of time than impulsive sources. In **Paper I**, a seismic vibrator driven by an electric linear synchronous motor (LSM or E-Vib) was used as the seismic source (Figure 3.7b). It consists of a baseplate connected to a coil sliding in between a U-shaped permanent magnet track (Brodic et al., 2021). This design allows production of a controllable force with low signal distortion. The bandwidth response of the E-Vib is 2-200 Hz with a flat amplitude. No internal hydraulic system is involved; hence no strong harmonics are generated in the data.

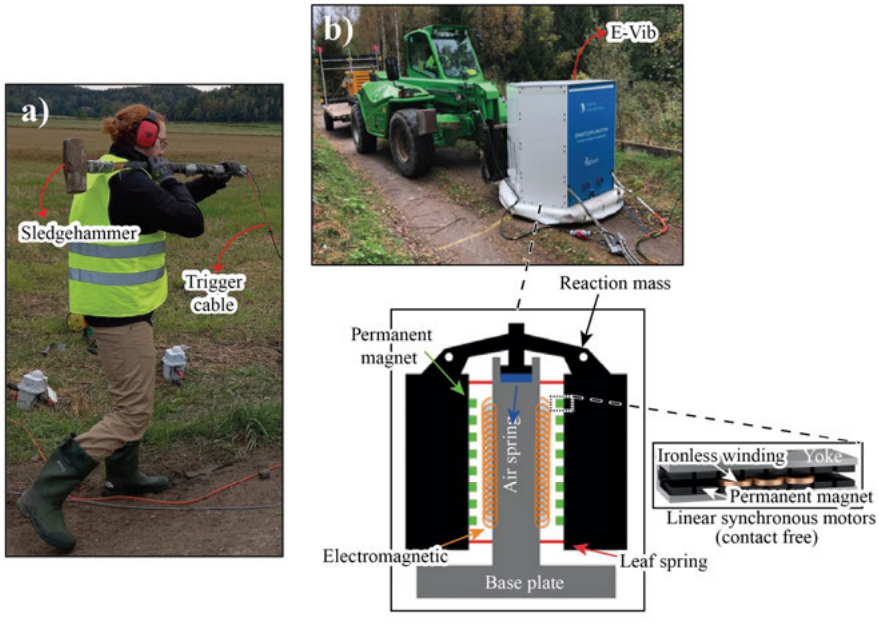

Figure 3.7. Different types of sources are used for the seismic acquisition in this thesis work. The (a) Sledgehammer (**Papers II** and **III**) and (b) E-Vib (**Paper I**) were used as seismic source.

4 Summary of papers

4.1 **Paper I:** Broadband seismic source data acquisition and processing to delineate iron oxide deposits in the Blötberget mine-central Sweden

The goals of the study in **Paper I** were, firstly, to test a prototype electromagnetic-based vibrator (E-Vib) for hardrock mineral exploration, and secondly, to image the mineral deposit from Blötberget mine in high resolution with focus on a broadband data processing workflow. The seismic data processing workflow helped to retain the broadband frequency while attenuating source-generated and ambient noise. The mineralization was successfully imaged, and a crosscutting-fault was suggested, supporting also results from previous studies in the area. The E-Vib proved its potential as a reliable seismic source for hard rock environments.

4.1.1 Synopsis

The need to evaluate the performance of new technologies, such as the E-Vib, in mineral exploration motivated a field campaign in 2019 along Profile 1 in the Blötberget area of Ludvika where earlier seismic studies using conventional seismic data acquisition setups were also available (Figure 4.1). Results from previous studies in Blötberget (e.g., Maries et al., 2017; Malehmir et al., 2017; Maries et al., 2020; Markovic et al., 2020; Malehmir et al., 2020 and 2021) highlighted this place as an excellent location for validation of different prototypes including the E-Vib. Seismic data were acquired in 2D using 128 wireless recorders and 425-cabled units connected to 10 Hz geophones with 5 m shot and receiver spacing for a total length of approximately 2.7 km. Shots were generated three times at every shot location and vertically stacked to improve the signal-to-noise ratio. The northern part of the profile was situated on a swampy road and in a forest, while the southern portion intersected a major road. However, the E-Vib demonstrated design advantages for its dimensions and adaptability to be used in all these challenging setups. Raw shot gathers presented strong surface waves, noisy portions on the southern part of the profile, but recognizable reflections from the mineralization (Figure 4.2).

A broadband processing workflow was developed and dealt with the seismic data characteristics to improve the resolution of the mineralization in the final seismic section.

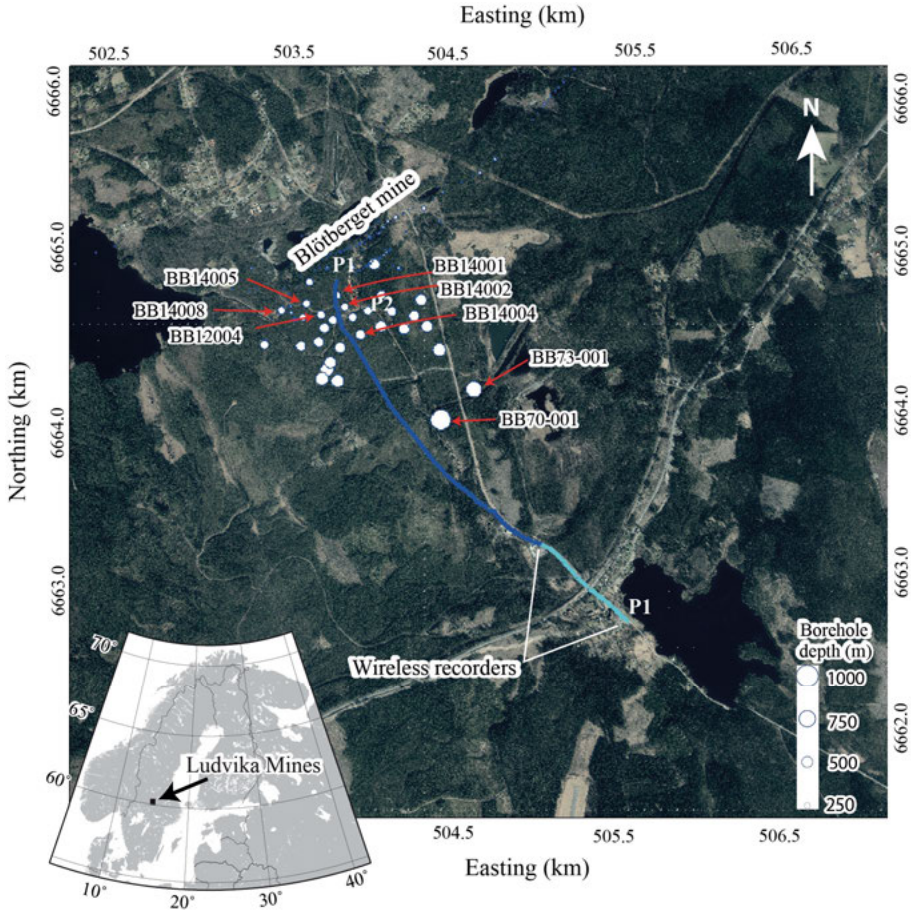

Figure 4.1. Aerial map of the study area in the Blötberget mine, part of the Ludvika Mines in central Sweden. The aerial photo shows the seismic profile, which portion of it was acquired with cabled receivers (dark blue line) and the other portion with wireless recorders connected to 10 Hz geophones (light blue line).

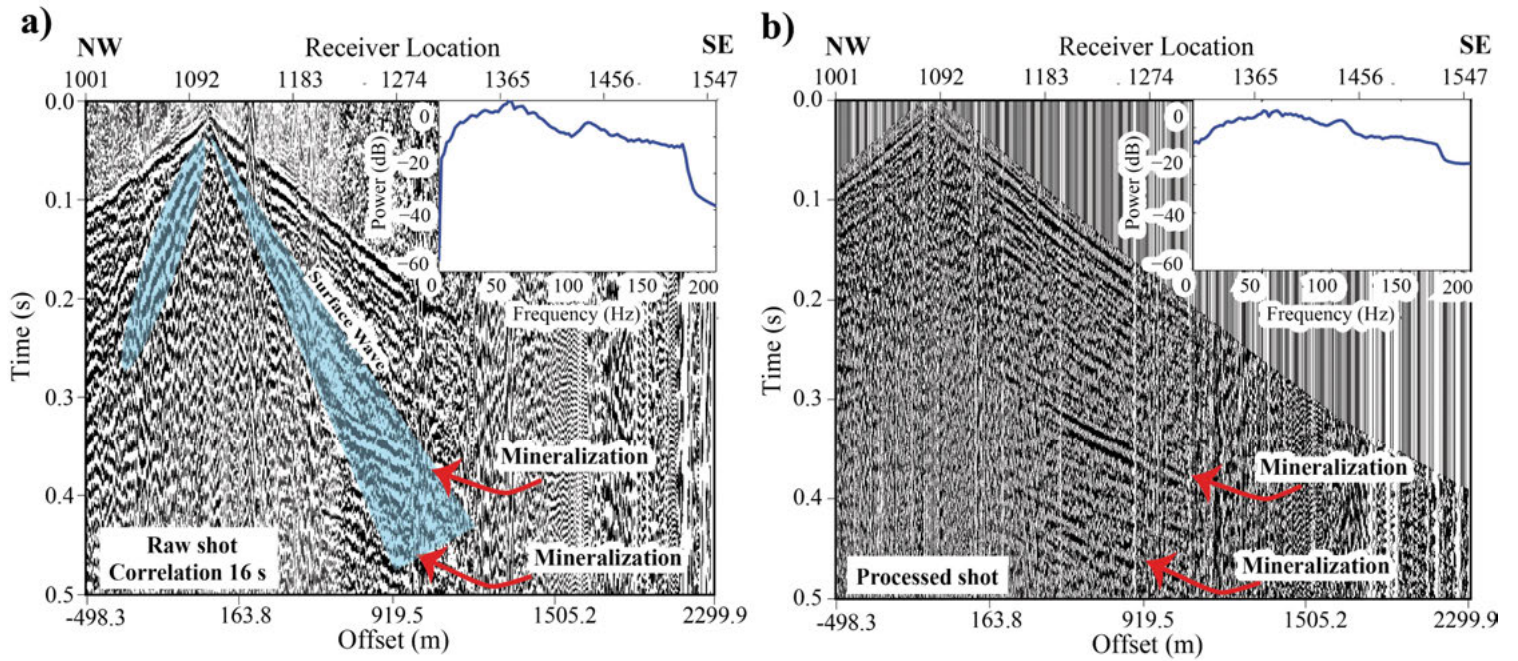

Figure 4.2. Shot gather example of the acquired data from the 2019 seismic campaign showing results of various processing steps performed in a tailored broadband processing workflow. (a) Raw shot gather showing strong surface waves (marked in the blue region) and (b) processed shot gather following the tailored broadband workflow. Reflections from the mineralization are labelled.

Unmigrated stacked sections, in Figure 4.3, image the mineralization (M1 and M2) and a deeper reflection (M3) previously also observed in the earlier studies (Maries et al., 2020; Markovic et al., 2020; Malehmir et al., 2021). A cross-cutting reflection (F1) dipping towards the northwest that was weakly observed in the earlier seismic campaigns (Figure 4.3a-c), appeared stronger with higher continuity and higher resolution in the E-Vib dataset (Figure 4.3d). Additionally, the possibility to compare different datasets along P1 acquired with different seismic sources, i.e., in this case drophammer and E-Vib, permitted in **Paper I** to analyze the potential of different sources for hardrock seismic applications. The comparison of the different seismic datasets, in **Paper I**, and inspection of the amplitude spectra revealed higher amplitude signals and increased frequency range when using the E-Vib, while a narrower frequency range was observed in the drophammer data.

Results in **Paper I** showed a high-quality migrated section obtained with the E-Vib (Figure 4.4). Borehole logging and models of the known deposits correlated well with the mineralization reflections and indicated a further extension at depth. The seismic section shows a deeper reflection, underlying the known deposits, likely indicating a probable mineralization.

4.1.2 Conclusions

The E-Vib, as a seismic source, contributed to the image enhancement of the hardrock subsurface. As an outcome, a broadband tailored workflow was developed that resulted in retaining the broadband frequency generated by the source. Stacked sections, migrated and unmigrated, imaged mineralized bodies and a fault system, previously speculated upon, but improved by the E-Vib source and the tailored broadband processing workflow. The analysis of different sources showed that the small side lobes of the wavelet signal, e.g., produced by the E-Vib, contribute to the resolution enhancement. **Paper I** supports the validation of new technologies in mineral exploration as a way to generate new knowledge and taking risks of testing new solutions in this field.

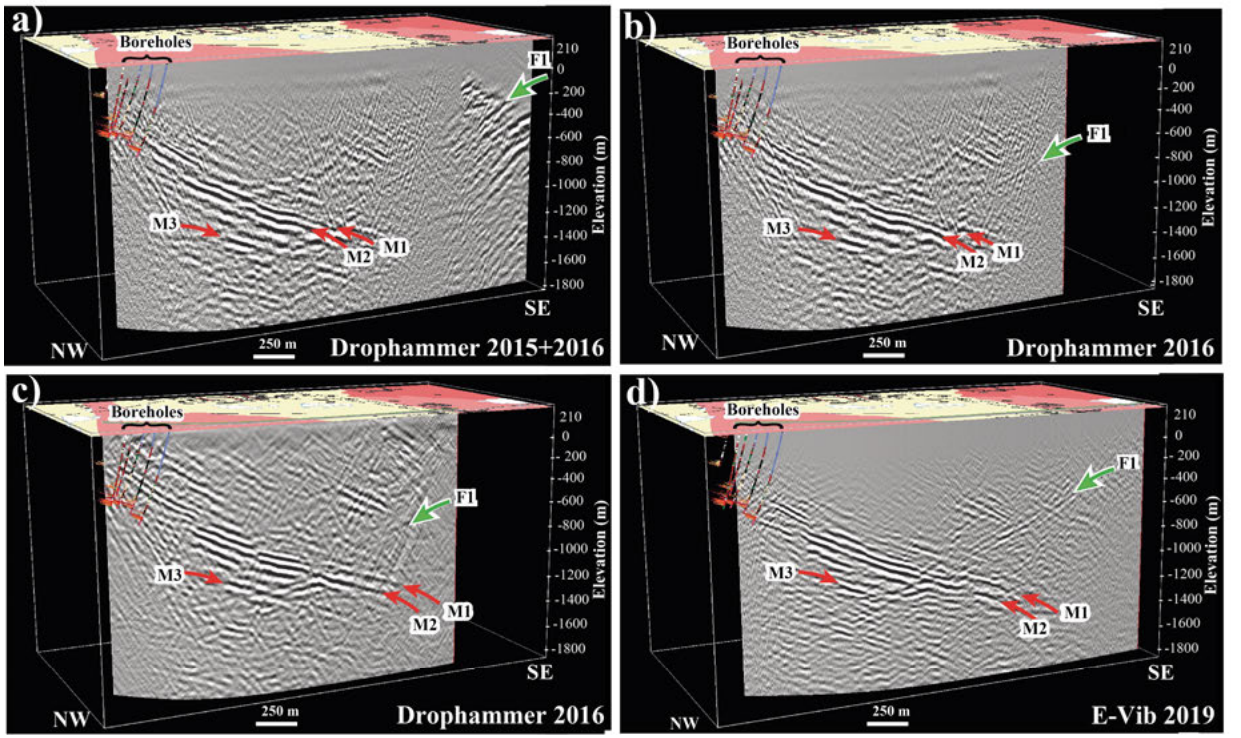

Figure 4.3. Unmigrated stacked sections of different seismic campaigns at Blötberget. (a) Unmigrated stacked section obtained from merging datasets from 2015 and 2016; (b) unmigrated stacked section from a 2016 survey using the drophammer seismic source; (c) the 2016 dataset section processed with the tailored broadband workflow from the E-Vib, and (d) section with the E-Vib as a source described in **Paper I**.

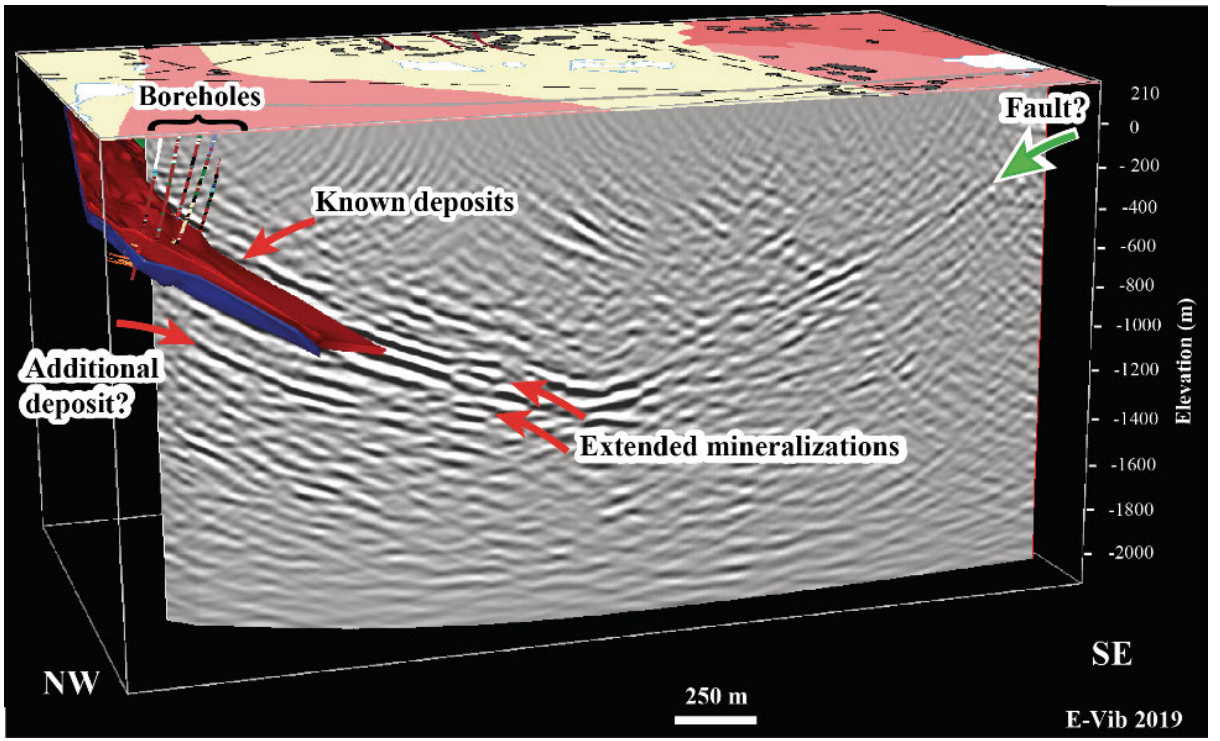

Figure 4.4. Migrated stacked section of the E-Vib dataset acquired for this campaign. Model of the known deposits (in red and blue), together with borehole logs, were correlated with the imaged reflections validating their origins. The section suggests a possible extension of the mineralization and probable additional resources underlying the known deposits. Additionally, the presence of a crosscutting reflection dipping from south to north was imaged in high resolution.

4.2 **Paper II:** Ultrahigh-resolution shear-wave reflection imaging of vertical-component data in a quick-clay prone to landslide area in southwest Sweden

Lilla Edet is a city located nearby Gothenburg city in southwestern Sweden (Figure 4.5). Geologically, this study area attracted attention because of the occurrences of landslides caused by quick clays. Consequently, several studies have been conducted to understand the geological structure, bedrock morphology and the presence of quick clays in the subsurface (Malehmir et al., 2013a, b; Lundberg et al., 2014; Salas-Romero et al., 2016, 2019, 2021). However, the clay conductivity limits the application of many geophysical methods like ERT, controlled-source and radio-magnetotellurics (Malehmir et al., 2013a), obstructing their depth penetration and resolution. While the gravity method can delineate bedrock topography, it is a low-resolution method with ambiguity hence seismic methods are favorable and can provide high-resolution images in highly conducted and saturated clays. **Paper II** deals with investigating the potential of ultrahigh-resolution seismic data in an area prone to landslide in the presence of quick clays, wherein strategy comprised finer-receiver sampling were used, and thus higher CMP-fold coverage than previous studies (Salas-Romero et al., 2019).

4.2.1 Synopsis

The ultrahigh-resolution seismic data were acquired near the city of Lilla Edet, near the Götaälv Zone, in southwestern Sweden (Figure 4.5). The Göta River is situated northwest of the profile, where on its north-eastern side a distinct landslide scar lies. A fixed spread of approximately 270 m long was acquired, bordered on both ends with bedrock outcrops. The 2D line benefited from 267 1C-wireless recorders with 1 m spacing and 240 shot points at nearly every receiver location. A 5-kg sledgehammer was used as the source and generated shots in both the vertical and horizontal directions. An additional roll-along dataset was acquired using a 3C-landstreamer and its results are presented in **Paper III**. This dataset supported whether the retrieved reflection wave modes from 1C-geophones in **Paper II** are of pure-shear origin by analyzing their particle motion hodograms.

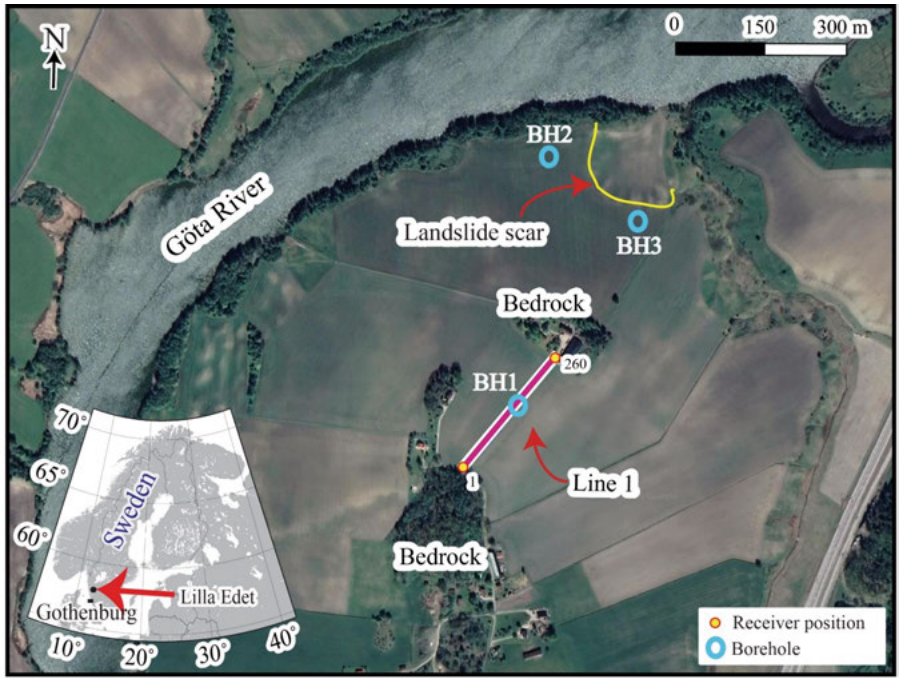

Figure 4.5. Aerial map of the study region, where the seismic line is situated in between bedrock outcrops, and near the Göta River, in Lilla Edet southwest of Sweden. A visible quick-clay landslide scar is observed northeast of the profile.

The survey recorded successfully high-quality shot gathers with notable first breaks for P- (red line in Figure 4.6a), S-waves (blue line in Figure 4.6c), and reflections marked by arrows (Figure 4.6). The processing was guided through a standard workflow to enhance P-P and S-S wavefield reflections, separately, and to attenuate surface waves. Figure 4.6b and d display the outcome of the main processing steps in the pre-stack stage, which included bandpass filter (BP) and spectral equalization (SPEQ).

The unmigrated stacked section presents strong reflections along the profile identified as S1, S2, and B. These reflections were later correlated with available logs, i.e., natural gamma and magnetic susceptibility, which identified two sets of coarse-grained layers as S1 and S2 and a crystalline bedrock as B. The P-P wavefield section shows a low resolution, and images S1 and the bedrock, but somewhat speculatively (Figure 4.7a). Given the slow S-wave velocity of the media, hence higher resolution for the S-S wavefield data, S2 is identified underlying S1 and the bedrock presents a complex undulated shape (Figure 4.7b). The bedrock morphology is confirmed by first break traveltime tomography results showing better resolution for the bedrock shape than the P-P wavefield reflection section. Outcomes from the first break traveltime tomography suggest P-wave velocities in a range of 1000-5000 m/s. Shear-wave traveltime tomography results suggest S-wave velocities on the

order of 50-200 m/s. The appearance of a series of diffraction signals within the S1 layer suggests local heterogeneities within the coarse-grained materials.

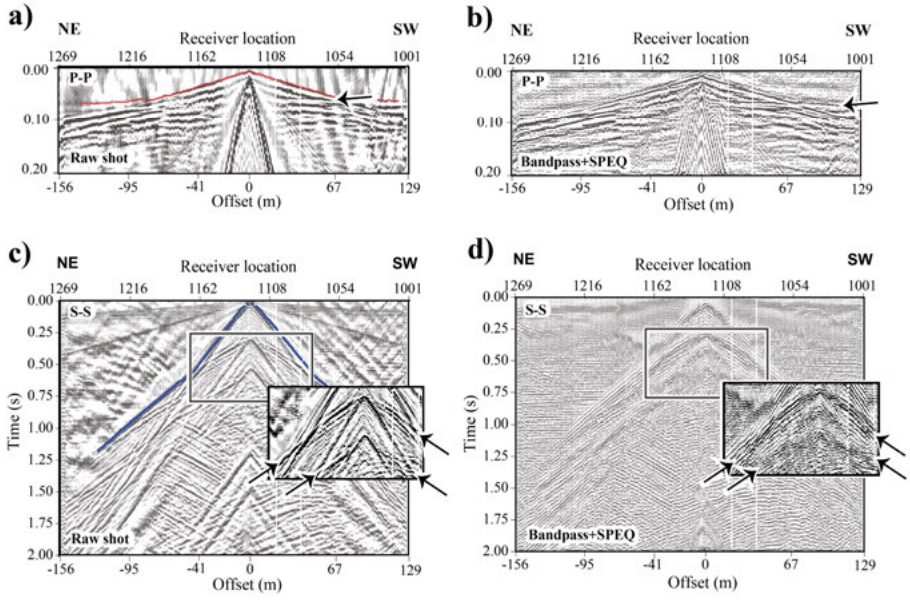

Figure 4.6. Shot gather example of the 1C seismic dataset through various processing steps of P-P (a-b) and S-S wavefield work (c-d). (a) Raw shot gather with first break picking for P-wave (marked in red). (b) Shot gather after processing steps showing P-P reflection. (c) Raw shot gather with S-wave picking (marked in blue) and a zoom into the S-wave reflections. (d) Denoised shot gather to enhance S-wave reflections. Arrows in the figure point at different reflections observed in the shot gathers.

As a complementary step, particle motion analysis was done on the 3C dataset to understand the origin of the observed reflections. It was applied trace-by-trace on the raw data on different parts of the shot gather such as first breaks, S-S wavefield reflections of S1 and B. It helped to identify that the polarization of the reflections is dominantly SV.

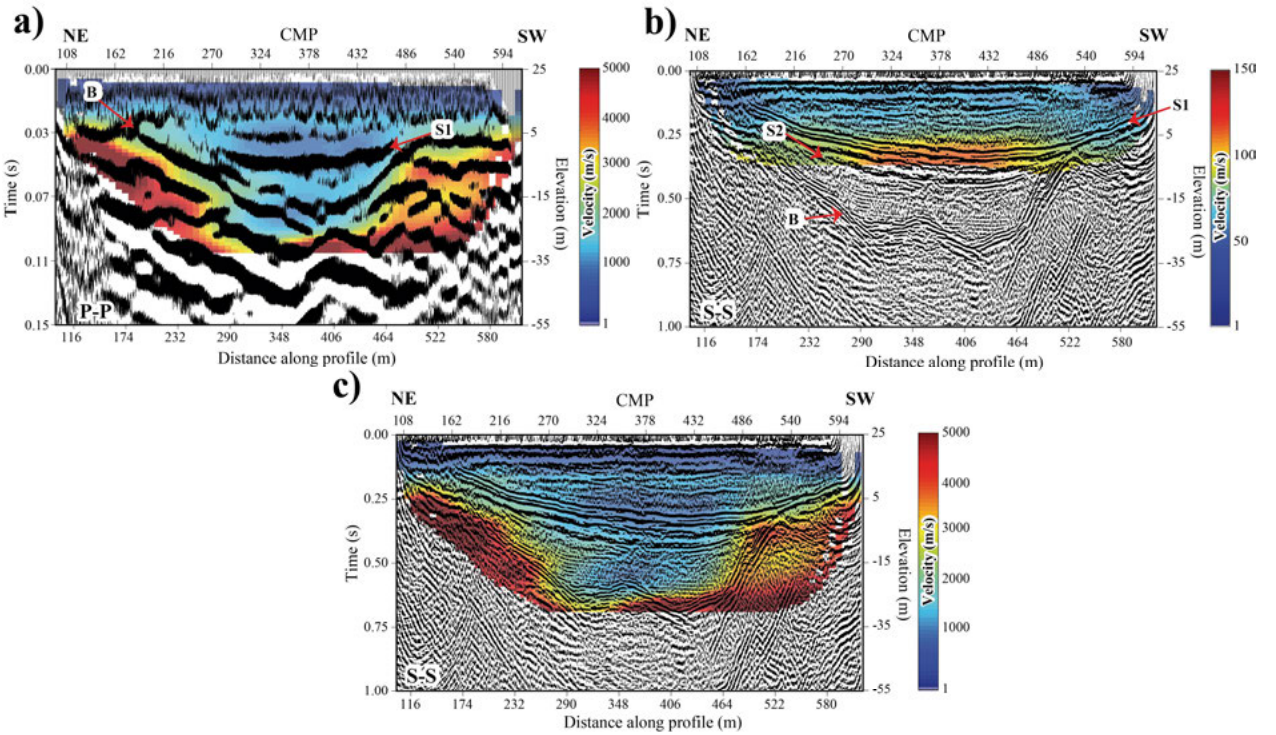

Figure 4.7. (a) P-P and (b) S-S wavefield unmigrated stacked sections of the same dataset with their respective traveltime tomography results overlapped for better interpretation purposes. (c) The first break traveltime tomography results superimposed on the S-S wavefield section showing good correlation between the two results. S1 and S2 are interpreted to be from coarse-grained materials while B from bedrock.

4.2.2 Conclusions

The 2020 seismic data acquisition permitted acquisition and imaging of the subsurface temporally and spatially less aliased, by retrieving shear-wave reflections from a vertical-component receiver and vertical component source setup. The P-P wavefield section in this high-contrast velocity setting provided depth control, together with borehole logs, of the imaged reflections. Nonetheless, the S-S wavefield section contributed to the detection of geological traits and soil conditions in greater resolution. The traveltime tomography for S-waves did not show deep penetration because of the slow velocities and relatively short offset. However, first break traveltime tomography results allowed imaging of the bedrock shape. A relatively high V_P/V_S ratio was observed, implying high-water content. This means higher probability of liquefaction in the region. Local heterogeneities, seen as diffractions during processing, are attributed to the presence of boulders in the coarse-grained layer. This facilitates the water flow within the strata and, hence, salt leaching from the clay and a probable liquefaction process when triggered.

4.3 **Paper III:** Ultrahigh-resolution 9C seismic survey in a landslide prone-area in southwest of Sweden

Paper III discusses the results of a 9C seismic data acquisition work recorded with a MEMS-based landstreamer system and a sledgehammer as the seismic source near the city of Lilla Edet along the same line shown in **Paper II**. This study reflects on the advantages of multicomponent seismic data acquisition in quick clay settings and the benefits they can provide compared to single component surveys.

4.3.1 Synopsis

The ultrahigh-resolution multicomponent seismic data acquisition was conducted in September 2020 near the city of Lilla Edet in southwestern Sweden along a 2D profile in a quick-clay landslide susceptible area (Figure 4.8). The dataset comprises a 120-m-long MEMS-based 3C-landstreamer with broadband frequency recording capability (0-800 Hz). It moved once to complete a 240 m long stretch of the entire profile. A 5-kg sledgehammer served as the seismic source, impacting over a metallic plate on vertical (V) and horizontal (HR and HT) directions at every receiver point with 1 m shot and receiver spacing. Due to the presence of slow wave-modes, the dataset was sampled by 1 ms with a record length of 3000 ms to ensure P-P and S-S wavefield reflections are retained down to bedrock, which was known from earlier studies and borehole data at approximately 50 m depth.

High fold and finer receiver and shot spacing as well as a super slow shear-wave velocity contributed to the ultrahigh-resolution seismic imaging at the study area. High-quality shot gathers were recorded, and strong hyperbolic reflections observed in all source-receiver orientations although with different quality and characteristics (Figure 4.9). Based on previous works and borehole logging data, two shallow reflections were identified as sandy-silty layers (S1 and S2), while a deeper reflection as crystalline bedrock (B).

The processing strategy aimed at only retrieving S-S wavefield reflections and followed a conventional workflow for every component of the 9C dataset. This helped to attenuate various types of noise while enhancing reflections. Each component was treated separately after vertical stacking of the repeated shot records, including a bandpass filter, spectral whitening, and an NMO velocity ranging from 1000-1500 m/s for P-P, and 60-120 m/s for S-S wavefields, respectively.

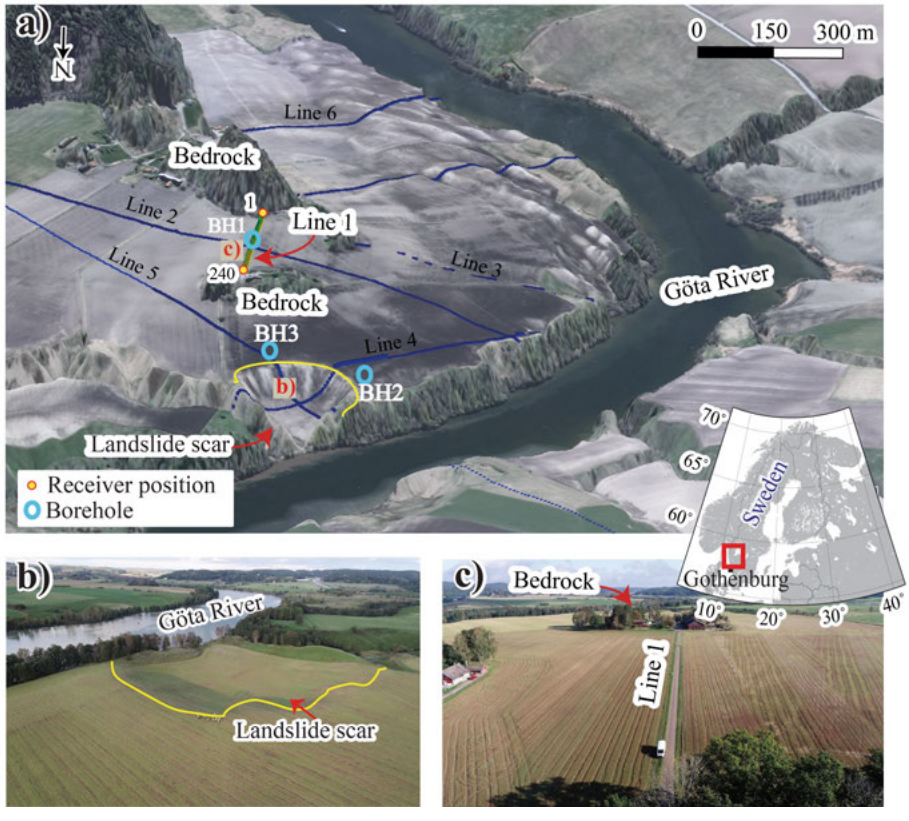

Figure 4.8. (a) Study area in Lilla Edet in southwest of Sweden, showing previous seismic lines (in blue) and the acquisition of line (Line 1) (in green). (b) A drone picture of the study area showing a clear quick-clay landslide scar (yellow zone) near the river, and (c) the seismic line bordered at its two ends with exposed bedrock.

Contrary to the P-P wavefield section (Figure 4.10a), which is better recorded in the V-V setup, the S-S wavefield sections present high resolution and provide detailed information on various structures within the clayey setting. The S-S wavefield image was optimally observed in the HT-HT and V-HT configurations (Figure 4.10a, b). To support this, radiation pattern plots were generated (Figure 4.10b, c). It is evident that P-wave energy is consumed by the presence of strong S-wave energy in this medium, supporting why S-S wavefield imaging is more favorable for quick-clay landslide studies than the P-P wavefield, or that at least a multicomponent survey should be attempted.

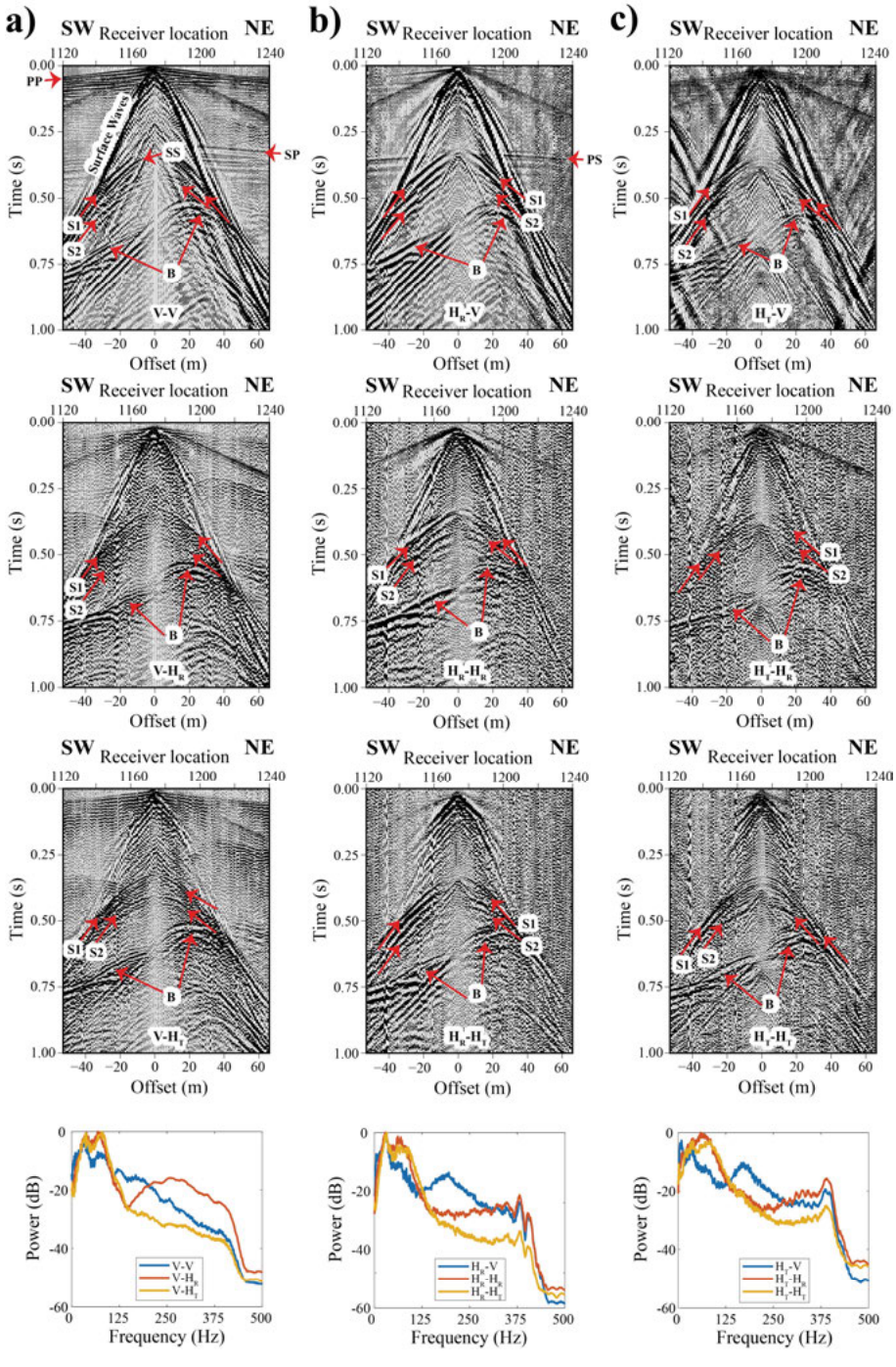

Figure 4.9. Example of a raw shot gather grouped at every column by source-orientation in vertical, horizontal, and transverse receiver-orientation: (a) vertical, (b) horizontal radial, and (c) transverse with their respective amplitude spectra.

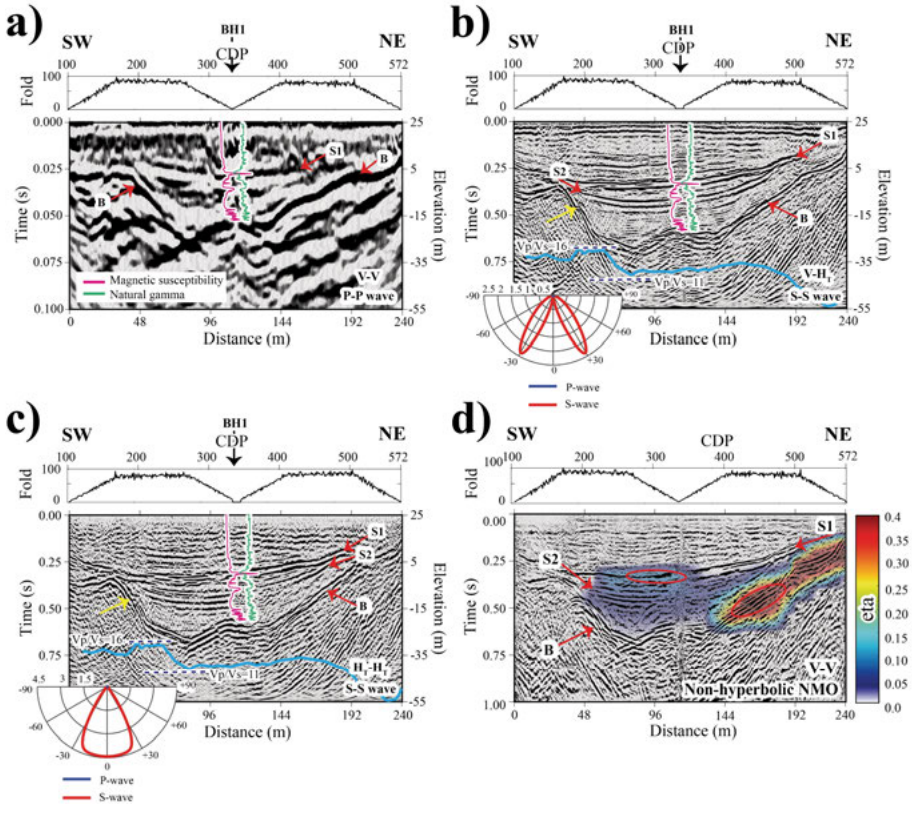

Figure 4.10. Optimal source-receiver orientation for P-P and S-S wavefields imaging from the 9C dataset; insets show estimated radiation patterns when using vertical and horizontal source-orientation. (a) P-P wavefield section using V-V configuration, (b) S-S wavefield section using V-HT and (c) HT-HT configurations. An eta parameter was included in the processing workflow in **Paper III**, which best improved S-S wavefield reflections obtained using (d) V-V configuration and identified portions with higher S-wave anisotropy.

Given the clay particle structure and high-sensitivity of shear-waves to an anisotropic medium (due to their smaller wavelengths), a non-hyperbolic fourth order moveout correction (NMO4) was included within the workflow and showed partial improvement in the S-S wavefield images, especially for vertical source-receiver orientation (Figure 4.10c). Figure 4.10c shows the overlapped eta parameter along the profile over the S-S wavefield section (V-V source-receiver orientation), allowing to identify portions where the eta parameter is different than 0 (when eta is greater than 0 means no anisotropy. See Alkhalifah and Tsvankin, 1995, and Thomsen, 1986). Eta parameter, or anisotropy value, ranges between 0.1 to 0.4 along the bedrock and S1

reflections and its inclusion helped to enhance the continuity of these reflections (marked in red circles in Figure 4.10d).

4.3.2 Conclusions

The acquisition of the ultrahigh-resolution 9C-seismic dataset showed to be beneficial for settings with the presence of quick clays, because of the completeness of information provided by different wave-modes recorded in different components. This kind of seismic dataset provides high-quality information for S-S wavefield imaging, in contrast to the P-P wavefield data, in clayey settings where water content is high. Despite the high-quality 9C seismic sections, the optimal source-receiver orientations for S-S wavefield imaging were V-HR and HT-HT configurations because they show higher quality reflections, especially for reflection S2.

Given the sensitivity of S-wave energy to anisotropy, it is advisable to study the wave propagation in all source-receiver setups, especially in media with high V_P/V_S ratio. Such a medium is favorable for S-S wavefield imaging because of clear shear-wave reflections and no source-generated noise cone of the shot records. In our case, the inclusion of non-hyperbolic moveout corrections in the processing workflow enhanced some of the reflections and helped to delineate zones with a higher degree of shear-wave anisotropy by including the eta parameter. Studying seismic anisotropy is quite innovative for quick-clay landslide studies and this can help to better understand clay structures and their water content, which is a step forward in delineating places where these sensitive clays are present. For the first time, **Paper III** reports such an attempt and the use of a 9C dataset for this purpose.

5 Future possibilities

During my PhD thesis work, several studies were additionally performed, but not presented in the second part of this thesis in the paper collection. Nevertheless, they may open opportunities to carry out more research and eventual publications for knowledge dissemination. This chapter is structured in two sections: transforming multiples into primaries using the seismic interferometric method and wavefield understanding.

5.1 Transforming multiples into primaries with interferometry

Most seismic studies focus on primary reflections and treating multiples as noise, hence targeting them as a primary noise for removal. However, multiples in their nature are secondary sources and can be used through seismic interferometry. Interferometry uses seismic wave interferences and recognizes patterns to determine earth properties (Berkhout and Verschuur, 2003; Schuster, 2009). In order to obtain a complete subsurface image, pairs of seismic traces should be correlated and summed over the source's boundary.

The method consists of analyzing the raypath from the source x to receiver A and B in the region of interest and turns one of the receivers into a virtual source position. For this to work, sources (x) and receivers are placed under the free surface (Figure 5.1a). If a multiple recorded in B, $G(B \shortmid x)$, is cross-correlated with the primary trace in A, $G(A \shortmid x)$, it can then be transformed into a redatumed primary recorded in B with a virtual source in A, $G(B \shortmid A)$, (Figure 5.1b). The following equation represents the Green's Function correlation of the raypaths repeated for every receiver along a profile at S_0' and all sources at S_0 (Schuster, 2009):

$$A, B \in S_0'; Im[G(B \shortmid A)] = k \int_{S_0} G(B \shortmid x)^* \, G(A \shortmid x) dx \quad (5.1)$$

The aforementioned equation is a reciprocity equation (Schuster, 2009) because one of the multiplication components is the complex conjugate of another (indicated by *).

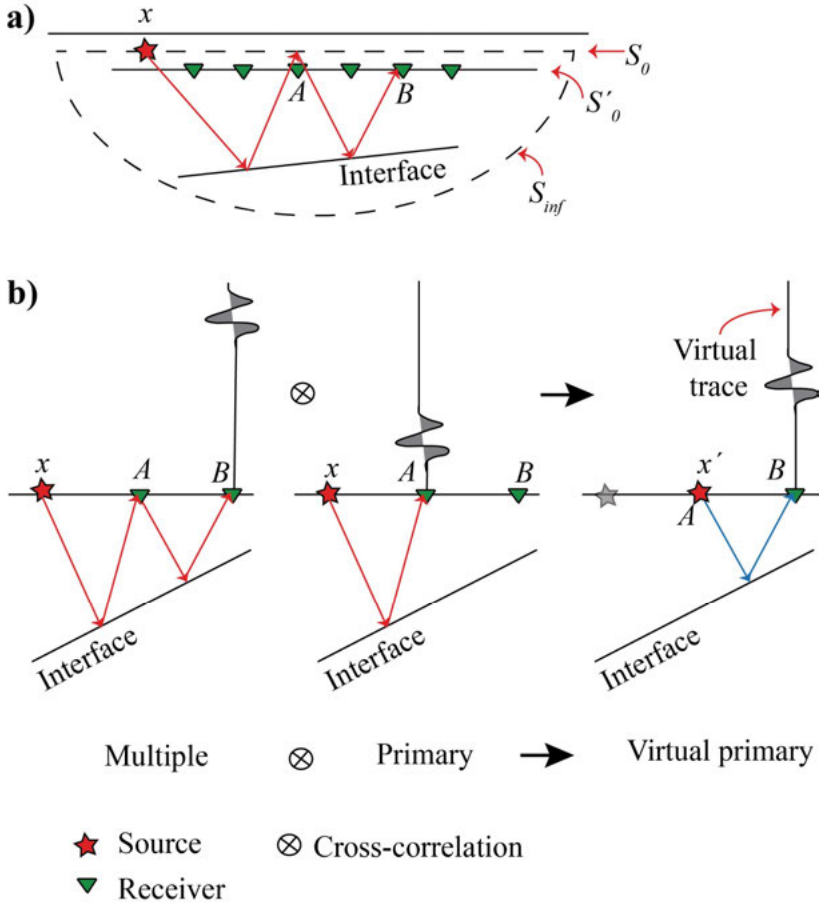

Figure 5.1. Transformation of multiples into primary events. (a) Geometry and array of receivers distributed on S'$_0$ line and sources along S_0 for the transformation. The area in the dashed line denotes the integration surface under a free surface. (b) Sketch representing events that contribute into the multiples transformation. x' is the virtual shot. Figure is adapted from Schuster (2009).

Data preparation was first done, as a first step, prior to the seismic interferometry on the 9C-dataset acquired from the Lilla Edet site. The seismic data used for this purpose is the S-S wavefield, but from the vertical source-receiver orientation, because of the presence of strong and visible multiples in this wavefield. The preparation steps included trace balancing and muting direct waves and reflections that did not interfere constructively. Therefore, a window was applied along the primary S-S reflections and their multiples to isolate them. At each shot gather, the primary in the trace at a selected receiver

A (red trace in the first panel of Figure 5.2a) was cross-correlated with the multiple in traces of receiver *B* (blue trace in the first panel of Figure 5.2a). The summation of all cross-correlated traces results in a virtual shot gather with the source placed at the position of receiver *A*. To obtain a complete virtual dataset, the aforementioned procedure should be repeated for all receivers along the profile (Wapenaar et al., 2010). The aim of the method is to obtain a dataset free of multiples and a final seismic section by the contribution of the correlation of primaries with their multiples.

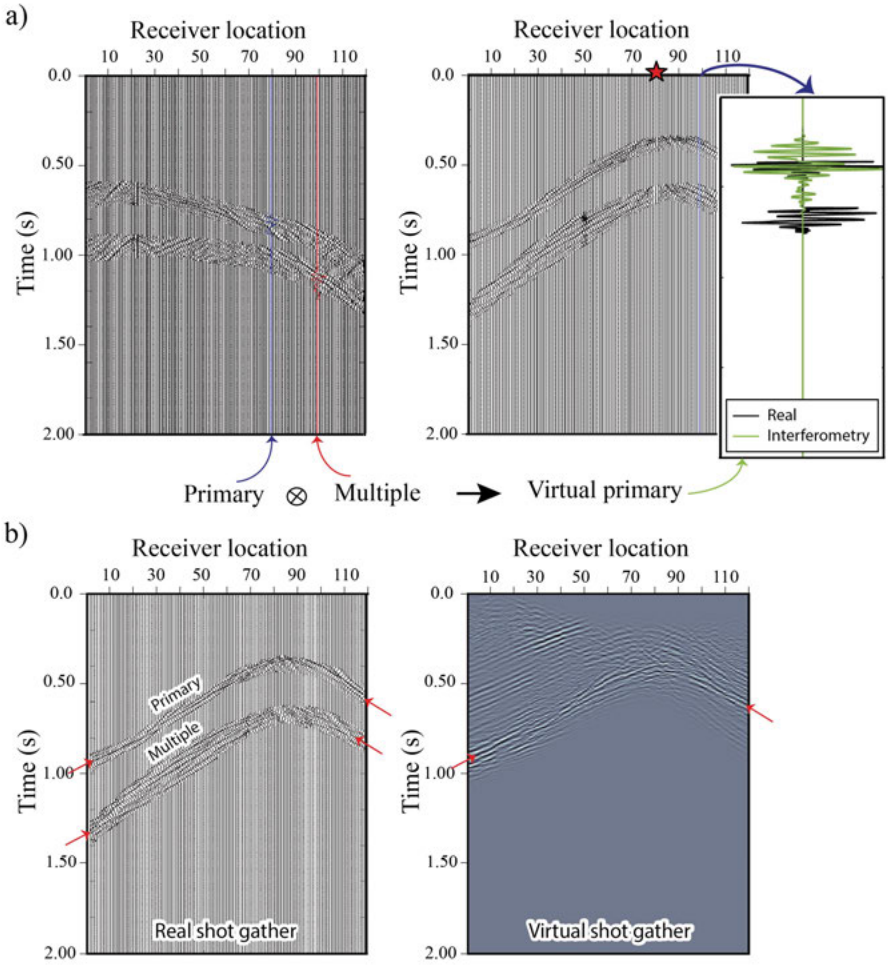

Figure 5.2. Example of transformation of multiples into primary events using V-V (vertical source-receiver orientation) dataset from the Lilla Edet site for (a) a trace and (b) a shot gather. (a) A multiple (red trace) was cross-correlated with the primary trace (blue trace) at two different receiver positions (shot gather to the left). The calculated virtual trace (green trace at inserted plot) corresponds to the virtual source position (red star) showing a match when compared with the real trace (black trace). (b) The real shot gather is compared to the virtual shot gather, which is obtained from the summation of the cross-correlated traces.

Comparing the virtual shot gather with the real shot gather, one observes that most of the primary events are encountered at the right position (Figure 5.2b). However, many artefacts are introduced in the virtual shot gather bringing up the challenges in the method. One key issue here is likely to account for the dipping effect of the layers. An attempt to apply this method was made and positive results were obtained on a few shot gathers. However, it failed on many parts of the profile with an increment of artefacts. Future attempts

should include the far-field approximation, which include the influence of dipping reflectors and the contribution of a Fresnel zone. This can open up possibilities for quick-clay studies and one way of reducing noise by utilizing the multiples.

5.2 Seismic modelling

Many approaches can be used to understand the wavefield of a wave propagating in the earth. The main objective is to predict different wave-modes recorded by receivers. This is a useful way to reconstruct the known initial conditions and simulate possible results. The techniques in this thesis are classified as direct methods, which means that they base their strategies on a geological model turned into a mesh, in which a forward problem is solved to generate data and to be compared with the actual observations. For this, a raytracing reflector modelling code and a finite-difference forward modelling code are used to help verify seismic interpretations.

5.2.1 Ray-trace modelling

The raytracing method approximates full wavefield modelling because they do not produce a complete wavefield from the modelling (Carcione et al., 2002). However, these methods are efficient and economical in computer resources. Raytracing consists of modelling traveltimes of reflections based on an initial given velocity model. The method includes a fan of rays shot in a 2D velocity model whose trajectories are solved for using the differential equations of rays on a spatial grid (Margrave, 2000). A starting point is determined first and traveltimes are calculated in constant time increments. The layers for this model are assumed flat, horizontal, and isotropic, which is a drawback for the current geological model because it contains a complex undulated bedrock in a bowl shape medium.

Figure 5.3 shows the modelled traveltimes superimposed onto the corresponding shot gather from the Lilla Edet dataset (V-V, vertical receiver-source orientation). Ray-trace modelled wave-modes P-P, S-P and S-S (blue, green, and red in Figure 5.3, respectively) for a source located at the receiver location 20 and recorded in an array of receivers along the profile with 1 m spacing are shown. The arrangement of sources and receivers for the traveltime calculations was determined with the same parameters as the real seismic data acquisition for the respective dataset. It was done with the purpose of comparing the real shot gather with the predicted reflection traveltimes.

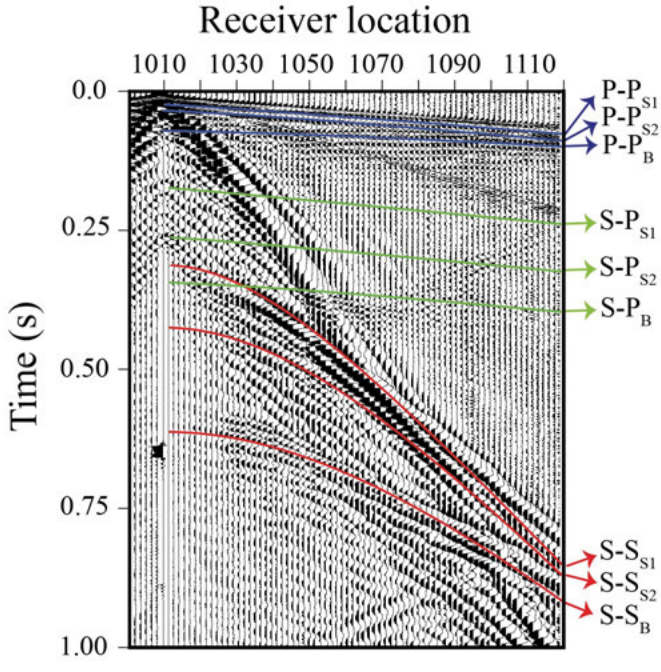

Figure 5.3. Calculated traveltimes superimposed onto a real shot gather from the Lilla Edet dataset. Traveltimes modelled different wave-modes observed in the V-V shot gather (vertical source-receiver orientation). P-P (blue line), S-P (green line) and S-S (red line) were calculated and matched with the identified reflections in the shot gather. But it was also possible to classify reflections from converted waves-modes, especially from the bedrock. In this figure S1 and S2 correspond to the sandy layers shallow and deep, respectively, and B is the bedrock.

Comparing the real shot gather with the modelled reflections, a good match is observed for the identified reflections. The wave-modes P-P and S-S reflections from S1, S2 and B (bedrock) horizons are observed and correlated as shown in Figure 5.3. However, the real shot gather could successfully record the S-P wave-mode from the bedrock but not visible from layers S1 and S2. Because a flat layering is assumed in the calculation of the traveltimes, a small mismatch at far-offsets especially for the S-wavefield reflections, is observed.

5.2.2 Synthetic seismograms using finite-difference (FD) forward modelling

Finite-difference (FD) modelling of wave propagation predicts through numerical methods what an array of sensors may register (Carcione et al., 2002). Synthetic seismograms are frequently generated to understand real seismic data and investigate a potential target. The finite-difference method solves the wave equation discretizing a geological model by a mesh in finite points. For

modelling wave propagation, we used the open-source code by Thorbecke et al. (2020). To avoid aliasing, the grid spacing (dx) should be properly constrained by the maximum source frequency (f_{max}) and minimum velocity (v_{min}), as following (Thorbecke et al., 2020):

$$dx \leq \frac{v_{min}}{2f_{max}} \tag{5.2}$$

Also, to assure convergence, the time step (Δt) of the numerical model is essential. The time step should be less than the time that the wave needs to arrive at an adjacent point grid of spacing. This is controlled by the stability conditions given by the following approximation (Thorbecke et al., 2020):

$$\Delta t < \frac{0.606\, dx}{v_{max}} \tag{5.3}$$

Absorbing boundaries are used to prevent reflections from the sides of the model and the top of the models are conditioned by a free surface. To develop the 2D-FD model, the geological and velocity models were reconstructed from the tomography results presented in **Paper II**.

Figure 5.4 shows resulting synthetic seismic data (left) modelled by elastic FD with conditions from the study area Lilla Edet and then compared with the real shot gather (right). The synthetic gathers modelled the reflections corresponding to S1, S2 and B. Traveltimes are consistent with the real data and show strong signatures of S-wave reflections. Figure 5.4a corresponds to a shot gather recorded in the vertical-component data. In this component, P-wave reflections (blue arrows) are identified at early times and correlate with the real shot gather. Figure 5.4b clearly shows the polarity flip recorded in the horizontal-component data given by the SV nature and it is also observed in the real data. This polarity flip was corrected during the processing steps of the real data. Converted wave-modes (green arrows) are well recorded in the horizontal-component data.

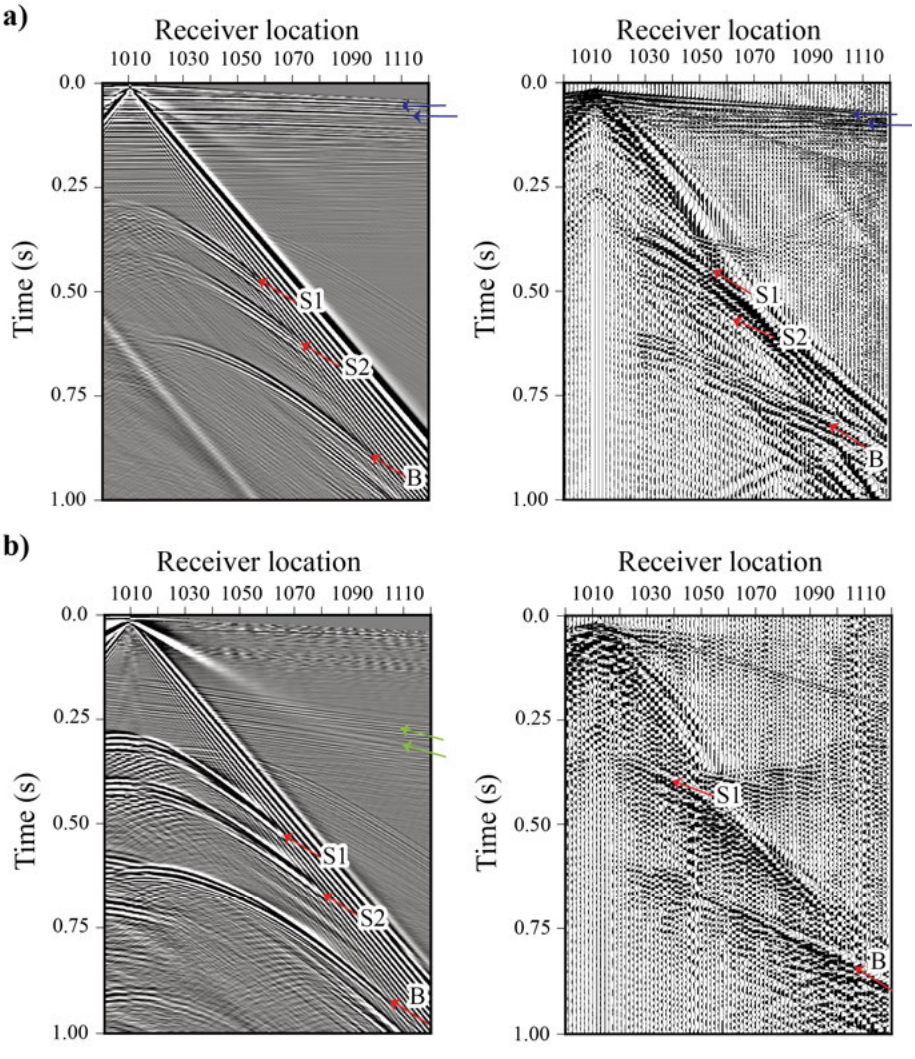

Figure 5.4. Synthetic shot gathers (left) modelled by 2D elastic finite-differences, using a vertical source, and recorded by (a) vertical- and (b) horizontal-component receivers and compared to a real shot gather example (right). P-wave reflections (blue arrows) are better identified in the vertical-component while converted wave-modes (green arrows) in the horizontal-component. S-wave reflections for S1, S2 and B are recorded in both of the components, but stronger signature is observed in the horizontal-component. However, S2 reflection is more difficult to identify in the real shot gather because of its proximity to reflection S1.

6 Conclusions

This PhD thesis work presents the benefits of seismic data acquisition for hardrock and over glaciofluvial deposits. Additionally, it illustrates the usefulness and completeness of seismic methods as a tool for various applications, in my case, in mineral exploration (**Paper I**) and for geohazards (**Papers II** and **III**).

In **Paper I,** the E-Vib was tested as a seismic source at the Blötberget Mine (Sweden) to validate its effectiveness and quality for the hardrock environment. The broadband source combined with a tailored processing workflow allowed imaging of reflections in improved resolution compared to the earlier seismic data. Seismic reflections corresponding to the iron-oxide mineralization were clearly delineated and a crosscutting reflection was imaged in high quality and fidelity. The reflections and the signature of the source in the seismic data were analyzed and compared with previous studies in the area to justify its effectiveness. The comparison showed a good correlation with the mineralized bodies detected before and indicated a higher resolution in the crosscutting reflection associated with a possible fault appearing to truncate the mineralization at depth. The sharper wavelet produced by the E-Vib analyzed on the first breaks and compared with the drophammer data acquired in the earlier studies indicated the potential of the E-Vib to acquire high-resolution seismic datasets. In this study the E-Vib showed its reliability as a seismic source in hardrock settings and for mineral exploration purposes. It was the first time it was tested for this purpose.

In **Paper II,** an ultrahigh-resolution shear-wave section, acquired in Lilla Edet (Sweden), was retrieved from vertical-component sources and receivers. Given the slow shear-wave velocity of the sediments in the area and the fine receiver spacing, a complex undulated bedrock and two coarse-grained layers interbedding clay deposits were imaged, and shear-wave reflections appeared less aliased compared to the earlier studies. As a complement to the seismic image, tomography results from first-break traveltimes of P- and S-waves provided medium velocities, showing surprisingly slow S-wave velocities on the order of 60-100 m/s. The analysis of particle motion on the reflections of the 3C dataset acquired at the same time confirmed an SV nature of the S-S wavefield reflections imaged in the V-V dataset.

Paper III further showcases studies done in the Lilla Edet area, but this time using a 9C seismic dataset acquired at the same time as the data presented in the latter study. Besides the ultrahigh-resolution S-S image, the 9C dataset allowed study of the wavefield complexity in the presence of quick clays. This analysis permitted us to identify the optimal receiver-source orientation to record P-P (V-V, vertical source-receiver orientation) and S-S wavefield (V-H_T, vertical source-orientation and horizontal transverse receiver-orientation, and H_T-H_T, Horizontal transversal source-receiver orientation) data in the area. Within the processing workflow, a non-hyperbolic normal-moveout was applied and allowed to include an anisotropy term. This improved the continuity of the reflections and identified regions of low-to-moderate degrees of anisotropy. As an outcome, a geological model was sketched illustrating the water flow, geological traits, and identified sections of partial collapse of clay structures, i.e., quick clays.

Results from these three articles of this thesis in two different geological settings open the possibility to further development works and testing of new methods and prototypes. For instance, from **Paper I,** it was worthwhile testing new technologies for seismic mineral exploration and developing efficient and cost-effective seismic methods for detailed imaging workflows. **Papers II** and **III** illustrate how seismic methods support characterizing zones of high risk for landslides and improved understanding of near-surface geology and physical conditions.

7 Sammanfattning på Svenska

Sverige ligger på den skandinaviska halvön, som är en del av den Fennoskandiska Skölden. Denna sköld är en av de tektoniska segmenten i den nordvästra delen av den Östeuropeiska kratonen. Majoriteten av den svenska berggrunden kom till under den Svekofenniska och den Svekonorska orogenesen.

Den svekofenniska orogenesen karaktäriserades av återkommande kratonkollisioner, vilket producerade subduktionszoner med magmatisk aktivitet, som ledde till formationen av magmatiska bergarter. De flesta av de malmförande bergarterna som finns i Bergslagen, Skellefteå och Norrbotten är produkter av aktiviteter från den Svekofenniska orogenesen. Det första studieområdet för denna avhandling är i Blötbergets gruva (Artikel 1), som är ett område som bildats under den Svekofenniska orogenesen. Detta studieområde finns i Bergslagen, som är känt för järnproduktion som bidragit till svensk ekonomi.

Lånt senare, under den kvartära tidsperioden, formades Sveriges landskap av den senaste glaciärens tillbakadragning och den efterföljande isostatiska anpassningen av landmassan. Detta förändrade utsträckningen av det som idag kallas Östersjön, och påverkade om leror och annat jordmaterial avsattes i marina eller lakustrina miljöer. I det andra studieområdet, Lilla Edet nära Göteborg (Artikel två och tre), har leror främst avsatts i marina miljöer, vilket har resulterat i en karaktäristisk "kvickhet". Dessa kvickleror blir lätt flytande när påverkande skjuvkrafter överstiger lerornas skjuvhållfasthet, vilket då leder till jordskred. På grund av djupet på dessa lerlager och deras förmåga att bli flytande innebär de en stor risk för infrastruktur, miljö och människor, då jordskred orsakar omfattande skador med stora sociala och ekonomiska kostnader.

Denna avhandling är uppdelad i sju kapitel och tre artiklar som är det samlade resultatet av mina doktorandstudier. Kapitel 1 introducerar forskningsämnet och de huvudsakliga målen. Kapitel 2 presenterar de studerade områdena tillsammans med geologiska beskrivningar, tidigare studier samt bergarternas fysikaliska egenskaper. Kapitel 3 ger en teoretisk bakgrund som är nödvändig för att förstå den vetenskapliga förankringen. Kapitel 4 sammanfattar de tre artiklarna som författats under doktorandstudierna. Kapitel 5 behandlar ämnen som är utanför begränsningen för denna avhandling men som belyser behoven

av framtida forskning. Slutsatserna för avhandlingen ges i kapitel 6, en sammanfattning på svenska och spanska ges efter det.

Denna avhandling inkluderar tre publicerade artiklar som författades om två studieområden. Artikel ett fokuserade på seismiska data från gruvan i Blötberget i Sverige, där en elektromagnetisk vibrator (E-Vib) testades för mineralprospektering i berggrund för första gången. Resultatet jämfördes med tidigare seismiska studier utmed samma profil där en mekanisk hammare använts som källa för stötvågor. Det två metoderna jämfördes och fördelarna med E-Vib som seismisk källa belystes.

Artikel två och tre handlar om samlade data från ett kvickleraområde i Lilla Edet i Sverige, den ligger i Sydväst och nära Göteborg stad, där anskaffning av data utfördes med 1C och 9C med låga mellanrum. Artikel två visar resultatet av ett dataset med ultrahög upplösning där skjuvvågor samlades in från 1C-geofoner. Resultaten möjliggjorde detaljerad avbildning av jordlagren och visade berggrundens komplexitet. Artikel tre visar fördelarna med en 9C anskaffning av data i kvickleraområden med risker för jordskred. Denna data visar vågornas komplexitet och bergarternas egenskaper som t ex anisotropi.

Denna avhandling utforskar möjligheten att använda nya typer av seismiska källor för mineralprospektering i berggrunden. Nya möjligheter öppnas upp för att använda skräddarsydda processeringsflöden för att behålla källsignaturen och också för att jämföra det med tidigare dataanskaffning för att belysa dess fördelar. Bredvid detta har seismiska metoder visats ha tillämpningar i sediment i jordskredskänsliga områden i Sverige. Denna forskning har underlättat förståelsen för kvicklera och hur seismiska metoder kan bidra till karaktärisering av denna typ av lera, samt vikten av att kontrollera känsliga jordarter.

8 Resumen en Español

El Escudo Fennoscándico que comprende a Suecia, ha sido formado por diferentes orogenias a lo largo del tiempo. Las orogenias Svecofeniana y Sveconoruega han influenciado la mayor parte del territorio. En la orogenia Svecofeniana ocurrieron procesos geológicos que dieron características de roca dura al subsuelo, favoreciendo así el origen de minerales como hierro, cobre, entre otros. El primer área de estudio en esta tesis (**Artículo I**), es la mina Blötberget, que se encuentra ubicada en la zona afectada por la orogenia Svecofeniana. Esta zona de estudio está en el distrito Bergslagen, caracterizada principalmente por la producción de hierro, el cual tiene gran participación en la economía de Suecia.

Mucho después de los procesos ocurridos en la orogenia Svecofeniana, aconteció la orogenia Sveconoruega formando la roca dura del suroeste de Suecia. Luego, en el periodo Cuaternario ocurrió el último tiempo glacial seguido del levantamiento isostático de tierra formando el paisaje en Suecia. Estos procesos hicieron que principalmente las arcillas fueran expuestas a medios de agua salina y fresca en periodos alternados. Debido a esto, las arcillas que predominan actualmente en esa zona, han tomado una característica de ´arcilla rápida´ en estado de gel casi lista para su licuefacción. Esta arcilla es sensible a fuerzas de cizallamiento y fácil de deslizarse. La segunda área en estudio (**Artículo II** y **III**) es en Lilla Edet, ubicada al Suroeste de Suecia, muy cerca de la ciudad de Gotenburgo. Esta zona es frecuentemente afectada por deslizamientos de tierra, afectando la población de la zona y la infraestructura civil.

Esta tesis tiene como motivación principal el uso de métodos sísmicos, para generar imágenes de subsuelo y así generar su respectiva caracterización. Los métodos geofísicos apoyaron la investigación del subsuelo sin técnicas invasivas. Los métodos técnicos, especialmente usados en esta tesis, aplican una metodología no destructiva maximizando estrategias medio ambientales.
En los **Artículos I, II** y **III** se discuten las ventajas del uso sísmico para roca dura, con enfoque en exploración minera y también en sedimentos suaves, en presencia de arcillas rápidas con tendencia a deslizamiento. Esta tesis de doctorado está enfocada a mostrar los beneficios de la adquisición sísmica y la innovación tecnológica en dos sitios en Suecia: la mina Blötberget (**Artículo I**) y Lilla Edet (**Artículos II** y **III**).

La tesis está estructurada en siete capítulos y tres artículos, como resultado de experiencias en mis estudios doctorales. El *capítulo 1* introduce los temas de investigación y principales objetivos. El *capítulo 2* presenta las áreas de estudio, incluyendo descripción geológica, estudios anteriores y propiedades físicas de la roca. El *capítulo 3* provee la teoría necesaria para entender el tema investigativo. El *capítulo 4* hace un resumen de tres artículos que fueron el resultado de investigación, durante mis estudios doctorales. El *capítulo 5* incluye los temas de la tesis que estuvieron fueron del límite investigativo, y que no fueron publicados en artículos, pero que resalta la importancia de su investigación a futuro. Las conclusiones son mencionadas en el *capítulo 6* y después se incluye un resumen en sueco y español.

Esta tesis incluye tres artículos publicados y desarrollados en dos áreas de estudio. El **Artículo I** se enfoca en información sísmica de la mina Blötberget en Suecia, donde se probó el vibrador electromagnetico (E-Vib) por primera vez en roca dura con propósitos de exploración minera. Los resultados fueron comparados con estudios sísmicos previos, hechos a lo largo del mismo perfil, usando el *drophammer* como fuente sísmica. Esta comparación fue hecha, mostrando ventajas sobre la información sísmica con el E-Vib y que presentaron mejores resultados frente a estudios anteriores.

Los **Artículos II** y **III** involucran información de Lilla Edet, Suecia, en el cual la adquisición de 1C y 9C con espaciamiento refinado, nunca antes visto, en un área con presencia de arcillas rápidas. El **Artículo II** muestra resultados de datos sísmicos de ultra resolución, donde las ondas de cizallas fueron extraídas de geófonos 1C. Los resultados permitieron generar imágenes detalladas del subsuelo y expone la complexidad de la base rocosa. El **Artículo III** exhibe las ventajas de la adquisición sísmica 9C en la región de arcillas rápidas con tendencia a deslizamientos. Esta data muestra su riqueza y revela la complejidad del campo de onda y propiedades de roca, tales como la anisotropía.

Aquí se estudia la posibilidad de usar nuevos tipos de fuente sísmica para roca dura con aplicaciones en exploración minera. La tesis genera oportunidades para incluir procesamientos de flujo que mantenga la frecuencia de banda y la naturaleza de la fuente. Esto fue comparado con adquisiciones previas para resaltar los beneficios de la implementación de este flujo de procesamiento. Además de eso, los métodos sísmicos muestran su aplicabilidad en sedimentos suaves en zonas de peligro en Suecia. La investigación apoya el entendimiento de las arcillas rápidas en Suecia y como los métodos sísmicos contribuyen al estudio y caracterización de este tipo de suelos, resaltando la importancia del monitoreo en suelos de alta sensibilidad.

9 Acknowledgements

I want to thank everyone who has been part of this journey. To my supervisor **Alireza** for the continuous teaching and sharing of experience that has helped me to grow.

To **Ayse** and **Chris** for their critical comments to improve my thesis.

Thanks to each professor that has contributed to my professional development from my bachelor to PhD studies. I learned a lot from each of you, from discipline to find my areas of interest.

Thanks to **Felix**! For your patience, support and advises. Thanks for sharing with me part of your life and studies since masters. All starting with when to take vitamin D and survive winter times in Germany. But also, the main learning is how to find time for a hobby! For your family that welcomed the warmest way ever. To your mom **Eva** for the sweet heart. To your siblings **Oskar**, **Agnes** and **Matilda**. To **Matilda** for always having an advice and a glass of wine.

To my colleagues **Zibi**, **Jolanta**, **Myrto**, **Magdalena**, **Samuel**, **Lea**, **Kristina**, **Mannos** and **Michael**. Special thanks to **Samuel** and **Zibi** for making me enjoying mentoring times. To **Samuel** for reading at the speed of light all the versions of my thesis until the last changed comma. For all the field works, a lot of teaching, patience and of course complaining that cannot be missed in you. To '*Ma boy*' **Zibi** for being the social soul and best officemate. You are always full of ideas and know how to make questions in the right time and correct words. But also, congratulations for the half marathon! Impressive change from the forever back pain boy to a professional runner. To my older brother, **Yinshuai**, for your advises and wise words. Always there for listening and lifting up words.

To all the geo students I met **Laura, Sebastian**, **Paula**, **Thorben**, **Michael**, **Andra**, **Taylor**. I shared different activities like gym, conferences, lunches, courses, and few TGIFs I shared. To **Thorben** and **Paula**, for the warm faces since day 1.

A mis padres, **Emiro** y **Nidia**, por el incondicional apoyo bajo cualquier circunstancia. Por las infinitas llamadas durante mis viajes de tren de regreso a casa. Que gracias a esas llamadas la distancia no nos separó. A **Felipe**, mi hermano, por su apoyo y tiempo de diversion en nuestras llamadas y nuestras esporádicas visitas. Finalmente, a la **JayJo** por sus podcasts mañaneros de consejos de belleza, temas climáticos, de cómo manejar el tiempo efectivamente y hasta de kuchen!

A mis amigos en Suecia por esas celebraciones de cumpleaños y reuniones de cafecito en nuestras casas. A los Guate, **Melanie** y **Luis**, a los Simons, **Simon** y **Carmen** y a nuestra querida **Rubí**. To **Dora** for her meetings at all kind of restaurants and her loud and contagious laugh!

Finally, I should say that a PhD journey is not easy, but it is worth it. All personal, professional, and technical grows will never leave from me.

Tatiana Pertuz,

Uppsala, February 2024

Seismic acquisition in Thorning (Denmark), August 2023.

References

Alkhalifah, T., & Tsvankin, I. (1995). Velocity analysis for transversely isotropic media. *Geophysics*, *60*(5), 1550–1566. https://doi.org/10.1190/1.1443888

Almqvist, B. S. G., Björk, A., Mattsson, H. B., Hedlund, D., Gunnarsson, K., Malehmir, A., Högdahl, K., Bäckström, E., & Marsden, P. (2019). Magnetic characterisation of magnetite and hematite from the Blötberget apatite – iron oxide deposits (Bergslagen), south-central Sweden. *Canadian Journal of Earth Sciences*, *56*(9), 948–957. https://doi.org/10.1139/cjes-2018-0183

Appelo, C. A. J., & Postma, D. (2004). *Geochemistry, groundwater and pollution*. CRC press.

Balestrini, F., Draganov, D., Malehmir, A., Marsden, P., & Ghose, R. (2020). Improved target illumination at Ludvika mines of Sweden through seismic-interferometric surface-wave suppression. *Geophysical Prospecting*, *68*(1), 200–213. https://doi.org/https://doi.org/10.1111/1365-2478.12890

Bergman, S. (2018). *Geology of the Northern Norrbotten ore province, northern Sweden*.

Berkhout, A. J., & Verschuur, D. J. (2003). Transformation of multiples into primary reflections. *SEG Technical Program Expanded Abstracts 2003*, 1925–1928. https://doi.org/10.1190/1.1817697

Bingen, B., Skår, Ø., Marker, Sigmond, Nordgulen, Ragnhildsveit, Mansfeld, J., Tucker, R., & Liégeois, J.-P. (2005a). Timing of continental building in the Sveconorwegian orogen, SW Scandinavia. *Norsk Geologisk Tiddsskrift*, *85*, 87–116.

Bingen, B., Skår, Ø., Marker, Sigmond, Nordgulen, Ragnhildsveit, Mansfeld, J., Tucker, R., & Liégeois, J.-P. (2005b). Timing of continental building in the Sveconorwegian orogen, SW Scandinavia. *Norsk Geologisk Tiddsskrift*, *85*, 87–116.

Bingen, B., Viola, G., Möller, C., Vander Auwera, J., Laurent, A., & Yi, K. (2021). The Sveconorwegian orogeny. *Gondwana Research*, *90*, 273–313. https://doi.org/10.1016/j.gr.2020.10.014

Bjerrum, L., & Rosenqvist, I. T. H. (1956). Some Experiments With Artificially Sedimented Clays. *Géotechnique*, *6*(3), 124–136. https://doi.org/10.1680/geot.1956.6.3.124

Bräunig, L., Buske, S., Malehmir, A., Bäckström, E., Schön, M., & Marsden, P. (2019). Seismic depth imaging of iron-oxide deposits and their host rocks in the Ludvika mining area of central Sweden. *Geophysical Prospecting*, *68*. https://doi.org/10.1111/1365-2478.12836

Brodic, B., Ras, P., de Kunder, R., Drijkoningen, G., & Malehmir, A. (2021). Seismic imaging using an e-vib — A case study analyzing the signal properties of a seismic vibrator driven by electric linear synchronous

motors. *Geophysics*, *86*(3), B223–B235. https://doi.org/10.1190/geo2020-0181.1

Buntin, S., Malehmir, A., Juhlin, C., & Malinowski, M. (2021). Seismic structure of the central Svecofennian lithosphere. In *Digital Comprehensive Summaries of Uppsala Dissertations from the Faculty of Science and Technology*. http://urn.kb.se/resolve?urn=urn:nbn:se:uu:diva-456619

Carcione, J., Herman, G., & ten Kroode, F. (2002). Seismic Modeling. *Geophysics*, *67*, 1304–1325. https://doi.org/10.1190/1.1500393

Cherry, J. T. (1962). The azimuthal and polar radiation patterns obtained from a horizontal stress applied at the surface of an elastic half-space. *Bulletin of the Seismological Society of America*, *52*(1), 27–36.

De Geer, G. (1940). *Geochronologia Suecica principles*. A&W.

Fällman, A.-M., Holby, O., & Lundberg, K. (2001). *Kolloiders betydelse för hållfasthet och föroreningstransport i jord*. Statens geotekniska institut.

Fjær, E., Holt, R. M., & Rathore, J. S. (1996). *Seismic Anisotropy* (E. Fjær, R. M. Holt, & J. S. Rathore, Eds.). Society of Exploration Geophysicists. https://doi.org/10.1190/1.9781560802693

Gaiser, J. (2016). *3C Seismic and VSP: Converted waves and vector wavefield applications*. Society of Exploration Geophysicists. https://doi.org/10.1190/1.9781560803362

Hardage, B. A., DeAngelo, M. V, Murray, P. E., & Sava, D. (2011). Multicomponent Seismic Technology. In *Geophysical References Series*. Society of Exploration Geophysicists. https://doi.org/doi:10.1190/1.9781560802891

Healy, D., Timms, N. E., & Pearce, M. A. (2020). The variation and visualisation of elastic anisotropy in rock-forming minerals. *Solid Earth*, *11*(2), 259–286. https://doi.org/10.5194/se-11-259-2020

Hloušek, F., Malinowski, M., Bräunig, L., Buske, S., Malehmir, A., Markovic, M., Sito, L., Marsden, P., & Bäckström, E. (2022). Three-dimensional reflection seismic imaging of the iron oxide deposits in the Ludvika mining area, Sweden, using Fresnel volume migration. *Solid Earth*, *13*(5), 917–934. https://doi.org/10.5194/se-13-917-2022

Hons, M. S., Stewart, R. R., Lawton, D. C., Bertram, M. B., & Hauer, G. (2008). Field data comparisons of MEMS accelerometers and analog geophones. *Leading Edge (Tulsa, OK)*, *27*(7), 896–903. https://doi.org/10.1190/1.2954030

Kathol, B., Serre, S. H., & Thomsen, T. (2020). *Provenance of Svecofennian sedimentary rocks in Bergslagen and surrounding areas*.

Khaldoun, A., Moller, P., Fall, A., Wegdam, G., De Leeuw, B., Méheust, Y., Otto Fossum, J., & Bonn, D. (2009). Quick Clay and Landslides of Clayey Soils. *Physical Review Letters*, *103*(18), 188301. https://doi.org/10.1103/PhysRevLett.103.188301

Krawczyk, C. M., & Polom, U. (2018). Detection of Mobile Quick-Clay Layers Using Shear Wave Reflection Seismics. In *Atlas of Structural Geological Interpretation from Seismic Images* (pp. 175–176). John Wiley & Sons, Ltd. https://doi.org/https://doi.org/10.1002/9781119158332.ch33

Laine, J., & Mougenot, D. (2014). A high-sensitivity MEMS-based accelerometer. *The Leading Edge*, *33*(11), 1234–1242. https://doi.org/10.1190/tle33111234.1

Lefebvre, G. (1996). Soft sensitive clays. *Special Report - National Research Council, Transportation Research Board*, *247*, 607–619.

Löfroth, H., Suer, P., Dahlin, T., Leroux, V., & Schälin, D. (2011). Quick clay mapping by resistivity–Surface resistivity, CPTU-R and chemistry to complement other geotechnical sounding and sampling. *Swedish Geotechnical Institute, Report GÄU*, *30*.

Lundberg, E., Malehmir, A., Juhlin, C., Bastani, M., & Andersson, M. (2014). High-resolution 3D reflection seismic investigation over a quick-clay landslide scar in southwest Sweden. *Geophysics*, *79*(2), B97–B107. https://doi.org/10.1190/geo2013-0225.1

Malehmir, A., Bastani, M., Krawczyk, C. M., Gurk, M., Ismail, N., Polom, U., & Perss, L. (2013a). Geophysical assessment and geotechnical investigation of quick-clay landslides–a Swedish case study. *Near Surface Geophysics*, *11*(3), 341–352.

Malehmir, A., Manzi, M., Draganov, D., Weckmann, U., & Auken, E. (2020). Introduction to the special issue on "Cost-effective and innovative mineral exploration solutions." *Geophysical Prospecting*, *68*(1), 3–6. https://doi.org/https://doi.org/10.1111/1365-2478.12915

Malehmir, A., Maries, G., Bäckström, E., Schon, M., & Marsden, P. (2017). *Deep targeting an iron-oxide ore body using a seismic landstreamer and a 500-kg drophammer source*. *2017*(1), 1–5. https://doi.org/https://doi.org/10.3997/2214-4609.201701416

Malehmir, A., Markovic, M., Marsden, P., Gil, A., Buske, S., Sito, L., Bäckström, E., Sadeghi, M., & Luth, S. (2021). Sparse 3D reflection seismic survey for deep-targeting iron oxide deposits and their host rocks, Ludvika Mines, Sweden. *Solid Earth*, *12*, 483–502. https://doi.org/10.5194/se-12-483-2021

Malehmir, A., Saleem, M. U., & Bastani, M. (2013b). High-resolution reflection seismic investigations of quick-clay and associated formations at a landslide scar in southwest Sweden. *Journal of Applied Geophysics*, *92*, 84–102. https://doi.org/https://doi.org/10.1016/j.jappgeo.2013.02.013

Margrave, G. F. (2000). *New seismic modelling facilities in Matlab*.

Maries, G., Malehmir, A., Bäckström, E., Schön, M., & Marsden, P. (2017). Downhole physical property logging for iron-oxide exploration, rock quality, and mining: An example from central Sweden. *Ore Geology Reviews*, *90*, 1–13. https://doi.org/https://doi.org/10.1016/j.oregeorev.2017.10.012

Maries, G., Malehmir, A., & Marsden, P. (2020). Cross-profile seismic data acquisition, imaging, and modeling of iron-oxide deposits: A case study from Blötberget, south-central Sweden. *Geophysics*, *85*(6), B233–B247. https://doi.org/10.1190/geo2020-0173.1

Markovic, M., Maries, G., Malehmir, A., von Ketelhodt, J., Bäckström, E., Schön, M., & Marsden, P. (2019). Deep reflection seismic imaging of iron-oxide deposits in the Ludvika mining area of central Sweden. *Geophysical Prospecting*, *68*. https://doi.org/10.1111/1365-2478.12855

Markovic, M., Maries, G., Malehmir, A., von Ketelhodt, J., Bäckström, E., Schön, M., & Marsden, P. (2020). Deep reflection seismic imaging of iron-oxide deposits in the Ludvika mining area of central Sweden. *Geophysical Prospecting*, *68*(1), 7–23. https://doi.org/https://doi.org/10.1111/1365-2478.12855

Maxwell, S. (2014). Microseismic Imaging of Hydraulic Fracturing. In *Distinguished Instructor Series*. Society of Exploration Geophysicists. https://doi.org/doi:10.1190/1.9781560803164

Miller, G. F., Pursey, H., & Bullard, E. C. (1954). The field and radiation impedance of mechanical radiators on the free surface of a semi-infinite isotropic solid. *Proceedings of the Royal Society of London. Series A. Mathematical and Physical Sciences*, *223*(1155), 521–541. https://doi.org/10.1098/rspa.1954.0134

Mitchell, J. K., Soga, K., & others. (2005). *Fundamentals of soil behavior* (Vol. 3). John Wiley & Sons New York.

Nordic Iron Ore (NIO). (2017). *Mineral Resource Estimate Report*. https://nordicironore.se/wp-content/uploads/2017/07/mineral-resource-estimate-update-2017_final.pdf

Osterman, J. (1963). Studies on the Properties and Formation of Quick Clays. *Clays and Clay Minerals*, *12*(1), 87–108. https://doi.org/10.1346/CCMN.1963.0120112

Pertuz, T., & Malehmir, A. (2023a). Ultrahigh-resolution 9C seismic survey in a landslide prone area in southwest of Sweden. *Geophysical Journal International*, *235*(3), 2094–2106. https://doi.org/10.1093/gji/ggad346

Pertuz, T., & Malehmir, A. (2023b). Ultrahigh-resolution shear-wave reflection imaging of vertical-component data in a quick-clay prone to landslide area in southwest Sweden. *Geophysics*, *88*(3), B121–B133. https://doi.org/10.1190/geo2021-0832.1

Pertuz, T., Malehmir, A., Bos, J., Brodic, B., Ding, Y., de Kunder, R., & Marsden, P. (2022). Broadband seismic source data acquisition and processing to delineate iron oxide deposits in the Blötberget mine-central Sweden. *Geophysical Prospecting*, *70*(1), 79–94. https://doi.org/10.1111/1365-2478.13159

Rankka, K., Andersson-Sköld, Y., Hultén, C., Larsson, R., Leroux, V., & Dahlin, T. (2004). *Quick clay in Sweden*. Statens geotekniska institut.

Rosenqvist, I. Th. (1966). Norwegian research into the properties of quick clay—a review. *Engineering Geology*, *1*(6), 445–450. https://doi.org/https://doi.org/10.1016/0013-7952(66)90020-2

Sadeghi, M., Morris, G. A., Carranza, E. J. M., Ladenberger, A., & Andersson, M. (2013). Rare earth element distribution and mineralization in Sweden: An application of principal component analysis to FOREGS soil geochemistry. *Journal of Geochemical Exploration*, *133*, 160–175. https://doi.org/https://doi.org/10.1016/j.gexplo.2012.10.015

Salas-Romero, S., Malehmir, A., Snowball, I., & Dessirier, B. (2019). Subsurface characterization of a quick-clay vulnerable area using near-surface geophysics and hydrological modelling. *Solid Earth*, *10*(5), 1685–1705. https://doi.org/10.5194/se-10-1685-2019

Salas-Romero, S., Malehmir, A., Snowball, I., Lougheed, B. C., & Hellqvist, M. (2016). Identifying landslide preconditions in Swedish quick clays—insights from integration of surface geophysical, core sample- and downhole property measurements. *Landslides*, *13*(5), 905–923. https://doi.org/10.1007/s10346-015-0633-y

Savko, A. D., Novikov, V. M., Boeva, N. M., Krainov, A. V, Milash, A. V, Zhegallo, E. A., Ovchinnikova, M. Yu., & Bortnikov, N. S. (2019). New Kaolin-Bearing Province of Russia in the Southern Part of the Voronezh Anteclise. *Doklady Earth Sciences*, *489*(2), 1417–1420. https://doi.org/10.1134/S1028334X19120225

Schuster, G. T. (2009). *Seismic Interferometry*. Cambridge University Press. https://doi.org/DOI: 10.1017/CBO9780511581557

SGU. (2023, January 24). *Ore production and trends*. https://www.sgu.se/en/mineral-resources/mineral-statistics/ore-production-and-trends/#:~:text=SGU%20annually%20collects%20detailed%20data,Swedish%20mining%20industry%20remained%20stable.

Shan, C., Bastani, M., Malehmir, A., Persson, L., & Engdahl, M. (2014). Integrated 2D modeling and interpretation of geophysical and geotechnical data to delineate quick clays at a landslide site in southwest Sweden. *Geophysics*, *79*, EN61–EN75. https://doi.org/10.1190/geo2013-0201.1

Shan, C., Bastani, M., Malehmir, A., Persson, L., & Lundberg, E. (2016). *Integration of controlled-source and radio magnetotellurics, electric resistivity tomography, and reflection seismics to delineate 3D structures of a quick-clay landslide site in southwest of Sweden*. https://doi.org/10.13140/RG.2.1.1388.1367

Söderblom, R. (1963). Some laboratory experiments on the dispersion and erosion of clay materials. *Proceedings of the Conference Held at Stockholm, Sweden, August 12-16*, *14*, 277.

Statistics of the Swedish Mining Industry 2021. (2022). https://resource.sgu.se/dokument/publikation/pp/pp202302rapport/pp2023-2-rapport.pdf

Stephens, M., Ripa, M., Lundström, I., Persson, L., Bergman, T., Ahl, M., Wahlgren, C.-H., Persson, P.-O., & Wickström, L. (2009). Synthesis of bedrock geology in the Bergslagen region, Fennoscandian Shield, south-central Sweden. In *SGU: Vol. v. 58*.

Talme, O. A., Wenner, C.-G., & Pajuste, M. (1966). *Secondary changes in the strength of clay layers and the origin of sensitive clays*. National Swedish Institute for Building Research.

Thomsen, L. (1986). Weak elastic anisotropy. *Geophysics*, *51*(10), 1954–1966. https://doi.org/10.1190/1.1442051

Thorbecke, J., Jbrackenhoff, & Koffieklopper. (2020). *JanThorbecke/OpenSource: Release for MME manuscript R2*. Zenodo.

Torrance, J. K. (2012). Landslides in quick clay. *Landslides: Types, Mechanisms and Modeling. Cambridge University Press, Cambridge*, 83–94.

Torrance, J. K., & Pirnat, M. (1984). Effect of pH on the rheology of marine clay from the site of the South Nation River, Canada, landslide of 1971. *Clays and Clay Minerals*, *32*, 384–390.

Tran, Q., Sołowski, W. T., Thakur, V., & Karstunen, M. (2017). Modelling of the quickness test of sensitive clays using the generalized interpolation material point method. In V. Thakur, J.-S. L'Heureux, & A. Locat (Eds.), *Landslides in sensitive clays* (pp. 323–336). Springer. https://doi.org/10.1007/978-3-319-56487-6_29

Wapenaar, K., Draganov, D., Snieder, R., Campman, X., & Verdel, A. (2010). Tutorial on seismic interferometry: Part 1 — Basic principles and applications. *Geophysics*, *75*(5), 75A195-75A209. https://doi.org/10.1190/1.3457445

Yehuwalashet, E., & Malehmir, A. (2018, September). *Gravity and magnetic survey, modeling and interpretation in the Blötberget iron-oxide mining area of central Sweden*. https://doi.org/10.1190/segam2018-2992225.1

Yilmaz, Ö. (2001). Seismic Data Analysis. In *Investigations in Geophysics*. Society of Exploration Geophysicists (SEG). https://doi.org/doi:10.1190/1.9781560801580

Acta Universitatis Upsaliensis

Digital Comprehensive Summaries of Uppsala Dissertations from the Faculty of Science and Technology 2349

Editor: The Dean of the Faculty of Science and Technology

A doctoral dissertation from the Faculty of Science and Technology, Uppsala University, is usually a summary of a number of papers. A few copies of the complete dissertation are kept at major Swedish research libraries, while the summary alone is distributed internationally through the series Digital Comprehensive Summaries of Uppsala Dissertations from the Faculty of Science and Technology. (Prior to January, 2005, the series was published under the title "Comprehensive Summaries of Uppsala Dissertations from the Faculty of Science and Technology".)

Distribution: publications.uu.se
urn:nbn:se:uu:diva-517419

ACTA UNIVERSITATIS
UPSALIENSIS
2024